

# Validation of Monte Carlo Event Generators for the Electron-Ion Collider

EIC-India, Software Working Group

June 2021

## 1 MC-data comparisons for the EIC

- Role of MCEG and need for validation
- Our approach: Comparisons to HERA data
  - data available for comparisons
  - overview of approach and structure of report
- Status of MCEG validation for the EIC

## 2 Tools

### 2.1 The Rivet framework for MC/data comparison

The Rivet [Bie+20b] package is in this report used for all validation against existing data, and is expected to be used for physics prediction for the EIC going forward, as the framework makes it easy to impose realistic experimental conditions on a Monte Carlo calculation. In this section we provide a brief description of Rivet, and refer to the manual cited above for a more detailed introduction.

The main purpose of the Rivet framework, is to allow for comparison to published data, under the same conditions as an experiment. An experimental analysis is often a very detailed and precise piece of work, and a brief description in a journal article, can seldom do the details full justice. Nevertheless, the details are important if the full utility of data is to be maintained even after an experiment has closed down, and the scientists responsible for the analysis have moved on. In Rivet, a data set is therefore published together with C++ code which reproduces the analysis on Monte Carlo simulated pseudo-data.

Technically, Rivet is a C++ library providing a) core functionality to write an analysis, and b) physics features which simplifies most standard operations carried out in analyses, as well as quite a few non-standard ones. On top of the framework, several (976 at the time of writing) analyses are written as plugin

libraries. Historically, Rivet has its origin in HZTool [Wau+06], a FORTRAN package developed to facilitate comparisons to HERA data. Even though some analyses have been ported from the old package,  $\mathcal{O}(100)$  ep analyses still exist exclusively in HZTool. An interface between the two is in its final stages of preparation, and the successful deployment of this is a high priority for the EIC software working group.

Rivet performs the analyses at what is colloquially called “particle level”. For data, this means that data should be unfolded. For Monte Carlo it means that no other information than what is provided in a HepMC [Buc+21] output file can be used in the analysis. This ensures that a Rivet analysis by construction will yield physical observables which, at least in principle, will be measurable by a detector experiment. Furthermore it ensures that a Rivet analysis is generator agnostic. Once a Rivet analysis is implemented, it can be used with any HepMC compatible event generator.

A good example of this feature, highly relevant for this report, is the treatment of DIS kinematics. In most cases, a DIS event includes an obvious candidate for the scattered lepton. Once selected, this lepton can be used to reconstruct the normal DIS kinematics variables. The event may, however, include other leptons, and in some cases it might not even be obvious which lepton was the “real” scattered lepton. In order to provide an accurate comparison, any ambiguity must be resolved without resorting to unphysical generator level event history. For this purpose, Rivet provides the `DISLepton` feature, which using a choice from the user, will provide a lepton selection equivalent to the experimentally used one.

Rivet includes several features like this, the user manual [Bie+20b] can be studied for examples, and ref. [Bie+20a] for a deeper introduction to heavy ion-specific features.

The output from Rivet is histogram files in the so-called `.yoda` format <sup>1</sup>. Rivet comes with a script which will easily plot the analysis output together with data. Several examples of such figures in their default configuration can be seen in this report. Experimental data is printed as black dots with attached error-bars, and one or several Monte Carlo curves can be overlaid, each with their own legend label. At the bottom a ratio plot (MC/data) for all the overlaid Monte Carlo curves is displayed. Rivet allows for statistically perfect run combination of parallel runs, using the script `rivet-merge` which is shipped with the program.

## 2.2 Herwig 7

Herwig 7 [1] is a general-purpose Monte-Carlo event generator which originated from the Herwig++ development and superseded the Fortran HERWIG series which terminated with HERWIG version 6. Herwig 7 exceeds the capabilities of HERWIG 6 and Herwig++ by far, but shares their philosophy in providing accurate predictions of QCD dynamics first and foremost for parton shower al-

---

<sup>1</sup>See <https://yoda.hepforge.org/> for an introduction

gorithms, but nowadays also extensively in improving the hard process through next-to-leading order QCD corrections and their combination with parton showers. Herwig 7 can handle electron-positron, electron-proton and proton-(anti-)proton collisions. Recent development has also focused on exploratory steps towards heavy ion collisions [1].

Herwig (we will skip the version number now), is providing two different parton shower modules based on complementary formalisms, one angular-ordered ('QTilde') algorithm reflecting the coherent branching method [2], and one which is based on dipoles ('Dipoles') stretched by colour charges [3]. The QTilde shower also includes QED radiation, something which will be available for the dipole shower in a future release. Both showers contain effects of heavy quarks in the quasi-collinear limit (e.g. see [4] for a comprehensive discussion), can handle decays of unstable coloured particles and keep track of spin correlations [5]. The dipole shower can also include some subleading-N suppressed contributions in the emission of soft gluons [6]. Both algorithms provide the weighted Sudakov veto algorithms to allow for some shower scale variations to be encoded as on-the-fly weights [7]. Several improvements on the logarithmic accuracy of Herwig's parton showers are underway.

Herwig can evolve hard scattering processes through a large library of builtin cross sections at the leading and next-to-leading order in QCD; it can also read in Les Houches event files. One of the major steps in the transition to Herwig 7 was the introduction of the Matchbox module [8], which interfaces to several external libraries such as MadGraph [9] and OpenLoops [10] to provide matrix elements, and assembles complete NLO QCD calculations including their matching to both parton shower modules following either the subtractive (MC@NLO-type) or multiplicative (Powheg-type) matching methods. It also delivers the ingredients relevant to multijet merging at NLO QCD following a unitarised scheme with the Dipoles shower [11]. Beyond-the-Standard-Model processes can be generated in a very flexible manner by Herwig through reading in a model file in UFO output. Herwig will then construct all production and decay modes allowed by the model and is able to simulate inclusive signatures, accounting for a broad range of tensor structures in the interactions [12].

Multi-parton interactions inside Herwig are modeled on basis of an Eikonal multi-parton interaction model [13] and now include a wide variety of improvements to account for soft and diffractive contributions [14] and the propagation of space-time information towards the hadronization model for an improved colour reconnection [15].

Hadronization in Herwig is by default possible using the Cluster hadronization model [16], though an interface to the string model is in preparation [17]. Colour reconnection is essential to allow the cluster model to account for baryon rates at hadron colliders, and to account for colour correlations among multiple scatterers in dense environments. Colour reconnection has been a focus of the non-perturbative development in Herwig in recent years [18] and shows close connection to the physics of colour-suppressed terms [19].

## 2.3 Pythia 8

Pythia 8 [Sjö+15] is a general-purpose Monte-Carlo event generator that replaced the old Pythia 6 almost a decade ago. At the beginning the main goal was to have a generator written in modern program language for the needs of LHC experiments including some new new features such as  $p_{\perp}$ -ordered parton shower (PS) that can be generated simultaneously with multiparton interactions (MPIs). Later on it has been extended to handle also other types of beam configurations and nowadays it exceeds Pythia 6 capabilities in most of the areas relevant for high-energy colliders.

For an electron-ion collider the most important recent developments include a new model for photoproduction, a version of the default parton shower that can handle DIS-type events [CS18] and a completely new parton-shower model DIRE [HP15] where DIS processes have been considered from the beginning. The latter was originally introduced as plugin but since 8.301 release it has become a part of the core program. In addition to mediating the recoil from parton-shower emissions to hadronic system keeping the outgoing lepton intact, it also includes the DGLAP splitting kernels at NLO making the evolution consistent with NLO PDFs. Also the phase-space will be correctly filled even in the region where the photon virtuality is not necessary the hardest scale thanks to properly-scaled evolution variable. Also the another new antenna-based shower model, VINCIA [Fis+16], can in principle be applied for DIS but so far tests have been sparse.

As the photoproduction framework covers also soft QCD processes, such as elastic scattering and diffraction, and has also a model for hard diffraction [HR19], large part of observables that can be measured in an EIC can now be simulated with Pythia 8. However, since most of the studies and tuning efforts so far have focused on LHC physics, the setup is still not quite as mature for electron-proton collisions and more tests and validations should be performed as is the goal of the studies reported in this document. However, a good agreement for different HERA data has already been demonstrated [Hel18].

There are also a couple of areas where more effort will be needed. One standing limitation is that DIS and photoproduction are handled in separate frameworks and thus it is not possible to smoothly combine these regions and generate events with an intermediate  $Q^2$ . Another important ongoing development is to combine the heavy-ion model Angantyr [Bie+18] in Pythia with the photon-induced processes to enable simulations also with a nuclear target [BR19]. Another foreseen avenue is to improve perturbative precision by setting up a NLO matching and merging for photoproduction and combine this with the NLO process in DIS.

## 2.4 Sherpa 2

Who will write this section?

### 3 Cross section comparison between Pythia6 and Pythia8

In this section, we use the Pythia model to simulate the ep collision with 275GeV for proton and 18GeV for electron. The Pythia program is a standard tool for the generation of high-energy collisions, comprising a coherent set of physics models for the evolution from a few-body hard process to a complex multihadronic final state. It contains a library of hard processes and models for initial- and final-state parton showers, multiple parton-parton interactions, beam remnants, string fragmentation and particle decays. It also has a set of utilities and interfaces to external programs. While previous versions were written in Fortran, Pythia 8 represents a complete rewrite in C++. The versions of PYTHIA6 is 6.4.28 and all improvements for ep collision are integrated[ref2]. Over the years we have implemented many changes to PYTHIA6 to correct some problems we found and to integrate some e-A physics. In this section, we didn't include the radiative corrections. The version of Pythia8 we use is pythia8301.

In order to do compare apples to apples, we used the same kinematic cuts in Pythia6 and Pythia8. Here we show the detailed setups for the cuts for Pythia6 and Pythia8:

- The minimum invariant mass:
  - CKIN(1)=1.0 ;
  - pythia.settings.parm("PhaseSpace:mHatMin",1.0);
- The minimum invariant pT:
  - CKIN(3)=1.624
  - pythia.readString("PhaseSpace:pTHatMin=1.624");
- Lower limit for invariant mass of photon-hadron:
  - CKIN(77)=5.0
  - pythia.readString("Photon:Wmin = 5.0");
- Minimum  $Q^2$ :
  - CKIN(65)=1.e-09
  - pythia.settings.parm("PhaseSpace:Q2Min", 1.e-09);
- Maximum  $Q^2$ :
  - CKIN(66)=2.
  - pythia.settings.parm("Photon:Q2max",2);

In Pythia8, the photoproduction interactions involves one or two photons, either in photon-photon or photon-hadron collision or photons emitted from lepton beams, includes both direct and resolved contributions and also soft QCD and MPIs for events with resolved photons. Only (quasi-)real photons are considered so virtuality of the photons is restricted. The upper limit for (quasi-)real photon virtuality is  $2GeV^2$ . So we only compare the cross section

Process	PYTHIA6 (mb)	PYTHIA8(mb)
f + f' ->f + f' (QCD)	3.098E-04	3.757E-04
f + fbar ->f' + fbar'	5.698E-06	6.111E-06
f + fbar ->g + g	7.085E-06	8.387E-06
f + g ->f + g	1.229E-03	1.824E-03
g + g ->f + fbar	1.823E-05	3.447E-05
g + g ->g + g	6.887E-04	1.456E-03
Elastic scattering	2.982E-03	4.084E-03
Single diffractive (XB)	2.127E-03	2.310E-03
Single diffractive (AX)	1.741E-03	2.676E-03
Double diffractive	1.192E-03	1.483E-03
Low-pT scattering	8.855E-03	
Non-diffraction		2.819E-02
q + gamma* ->q ( 0<Q2<2)	1.717E-02	
q + gamma* ->q (Q2 >10)	6.919E-05	6.495E-05
f + gamma*_T ->f + g	1.338E-04	2*1.618E-04
f + gamma*_L ->f + g	1.696E-07	
g + gamma*_T ->f + fbar	4.043E-04	2*3.859E-04
g + gamma*_L ->f + fbar	4.725E-06	

for  $Q^2 < 2GeV^2$  for most of the subprocesses. However for the LO DIS ( $q + \gamma^* \rightarrow q$ ), the Pythia8 can only handle high  $Q^2$  case, so we compare LO DIS only for  $Q^2 > 10GeV^2$ .

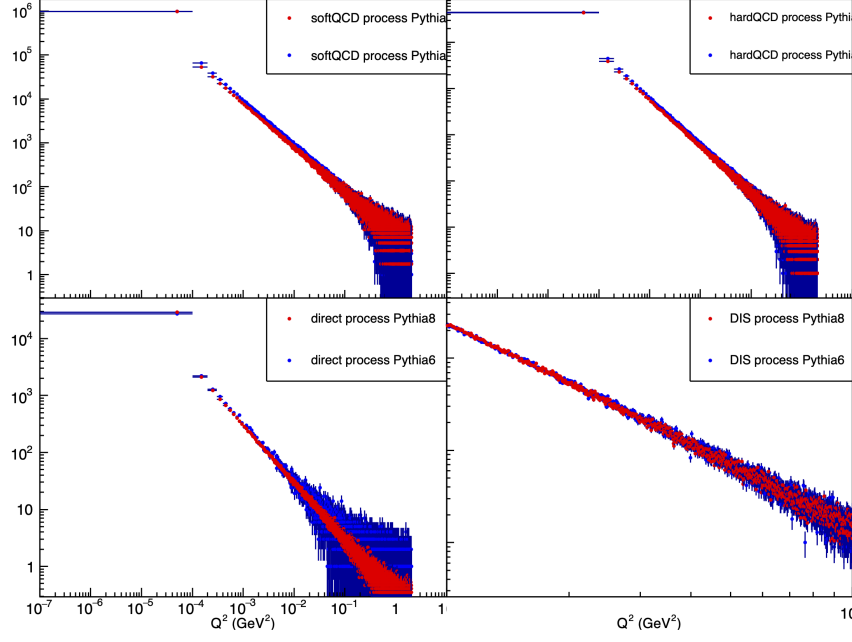


Figure 1:  $Q^2$  distribution for different subprocesses. For the LO DIS process,  $Q^2 > 10 \text{ GeV}^2$ . For other processes,  $10^{-9} \text{ GeV}^2 < Q^2 < 2 \text{ GeV}^2$ .

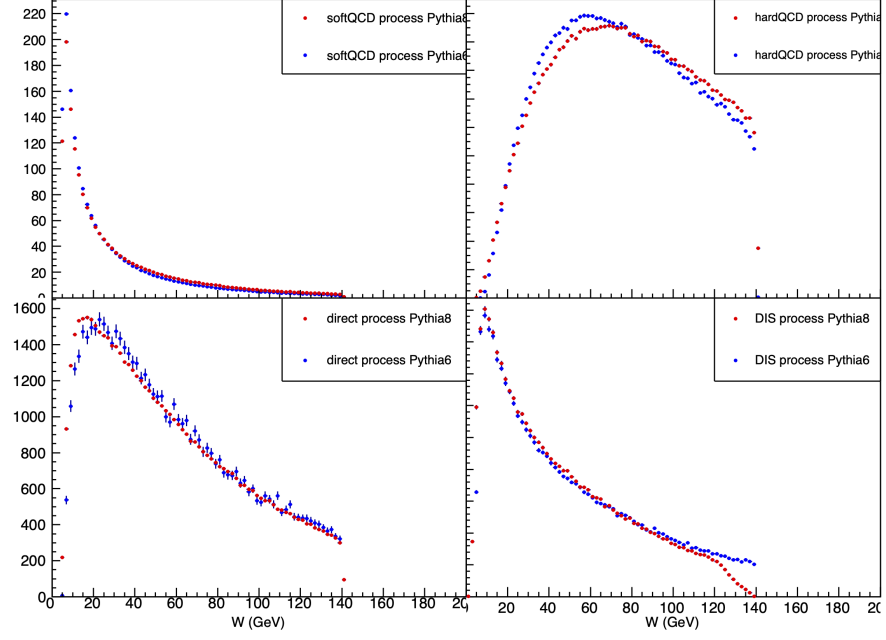


Figure 2: The  $W$  distribution for different subprocesses. For the LO DIS process,  $Q^2 > 10 \text{ GeV}^2$ . For other processes,  $10^{-9} \text{ GeV}^2 < Q^2 < 2 \text{ GeV}^2$ .



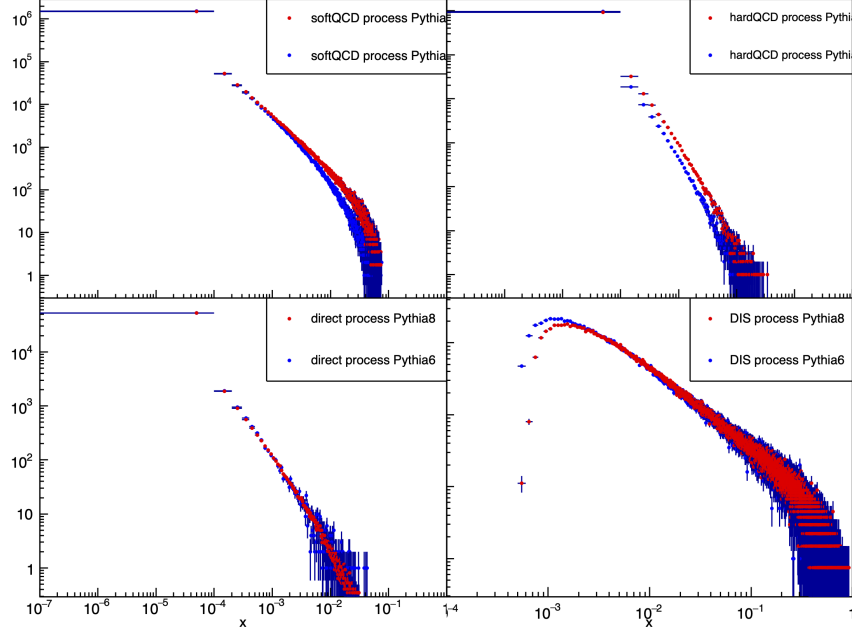


Figure 3: The  $x$  distribution for different subprocesses. For the LO DIS process,  $Q^2 > 10 \text{ GeV}^2$ . For other processes,  $10^{-9} \text{ GeV}^2 < Q^2 < 2 \text{ GeV}^2$ .

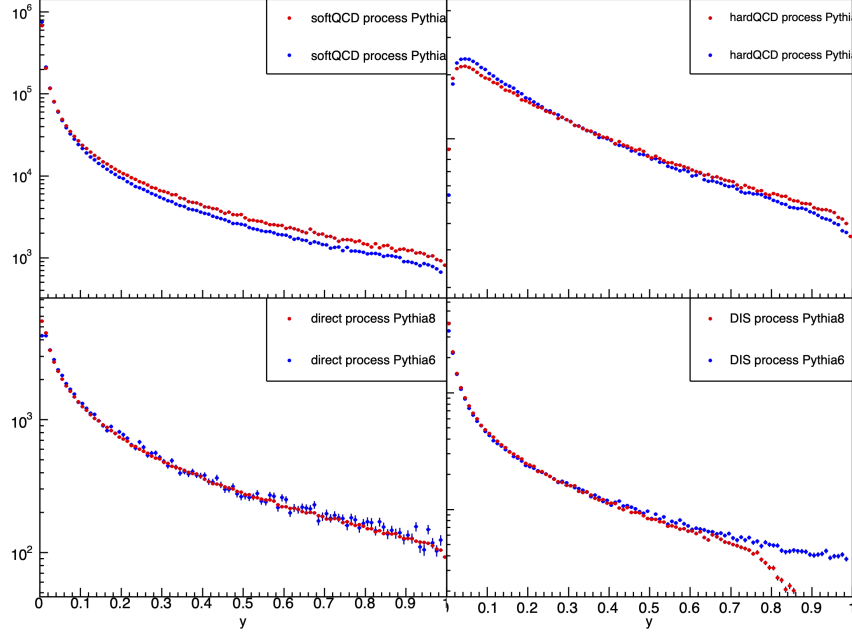


Figure 4: The  $y$  distribution for different subprocesses. For the LO DIS process,  $Q^2 > 10 \text{ GeV}^2$ . For other processes,  $10^{-9} \text{ GeV}^2 < Q^2 < 2 \text{ GeV}^2$ .

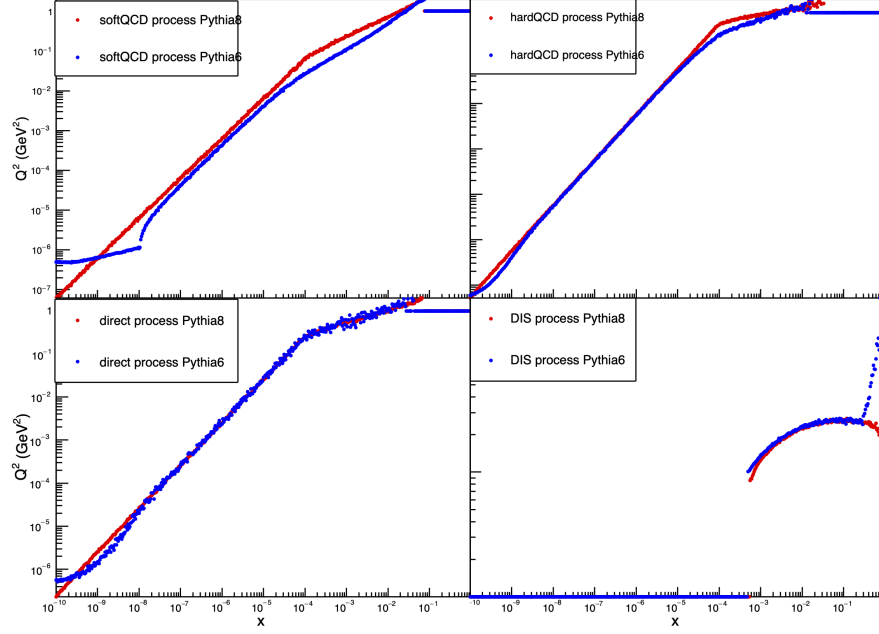


Figure 5: The  $Q^2$  vs.  $x$  distribution for different subprocesses. For the LO DIS process,  $Q^2 > 10 \text{ GeV}^2$ . For other processes,  $10^{-9} \text{ GeV}^2 < Q^2 < 2 \text{ GeV}^2$ .

## 4 Comparison Plots

List of our studies

## 4.1 Energy Flow and Charged Particle Spectra

Following data is presented in this subsection:

- Transverse Energy Flow in low and high  $Q^2$  region.
- Transverse Energy-Energy correlation in low and high Bjorken  $x$  region.
- Average Transverse Energy in Central and Forward region.
- Scaled Charged Particle Spectra.
- Average  $p_T^2$  distribution.

Pythia8, Sherpa2 and Herwig7 Monte Carlo generators are used.

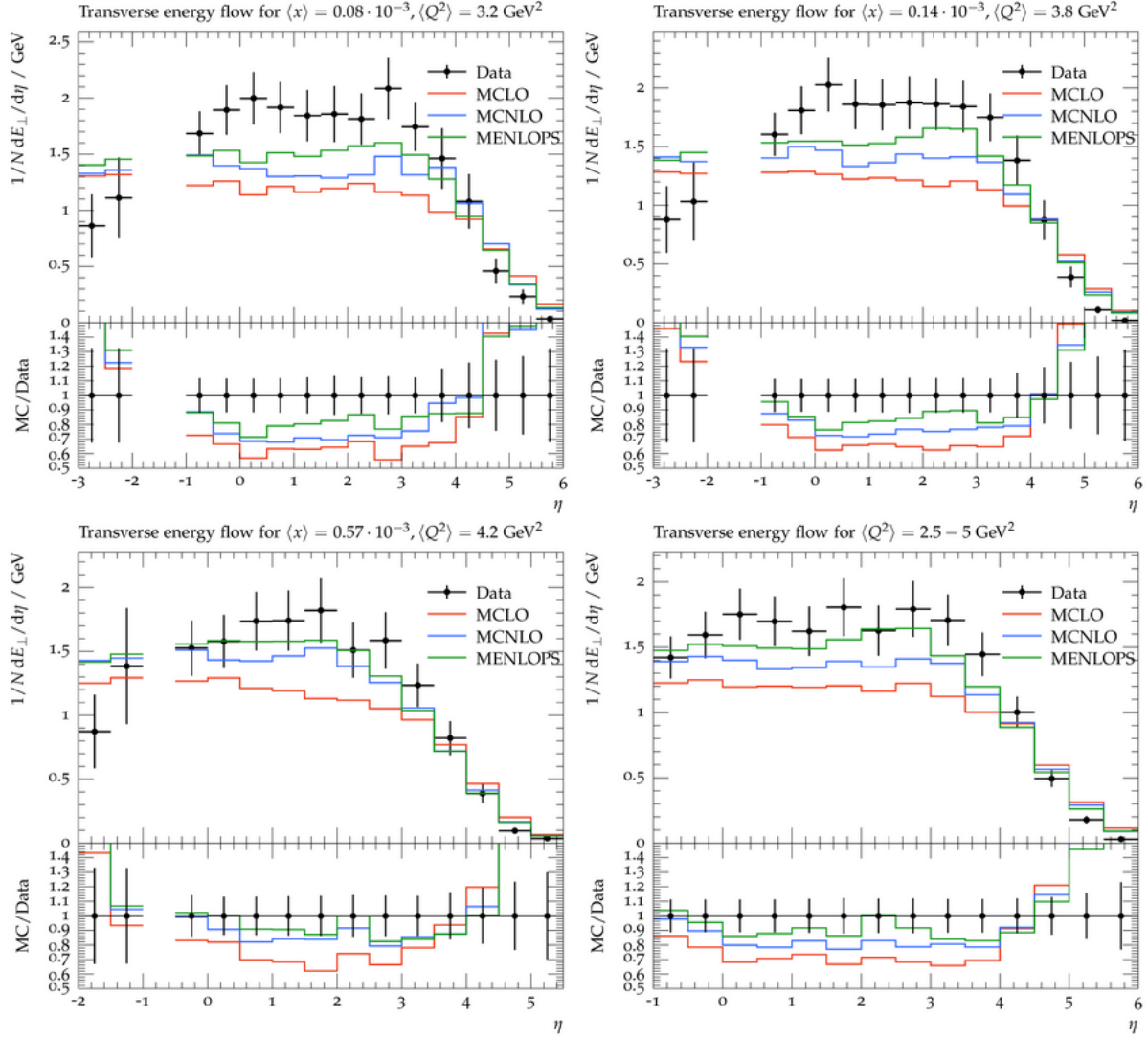


Figure 6: Sherpa2, 1M events, Beam energies-  $p = 820 \text{ GeV}^2, e = 27.5 \text{ GeV}^2$ . **Low  $Q^2$  region** is affected by saturation which arises when the photon wavelength is comparable to size of proton. In this region the transition from photo-production to DIS takes place.

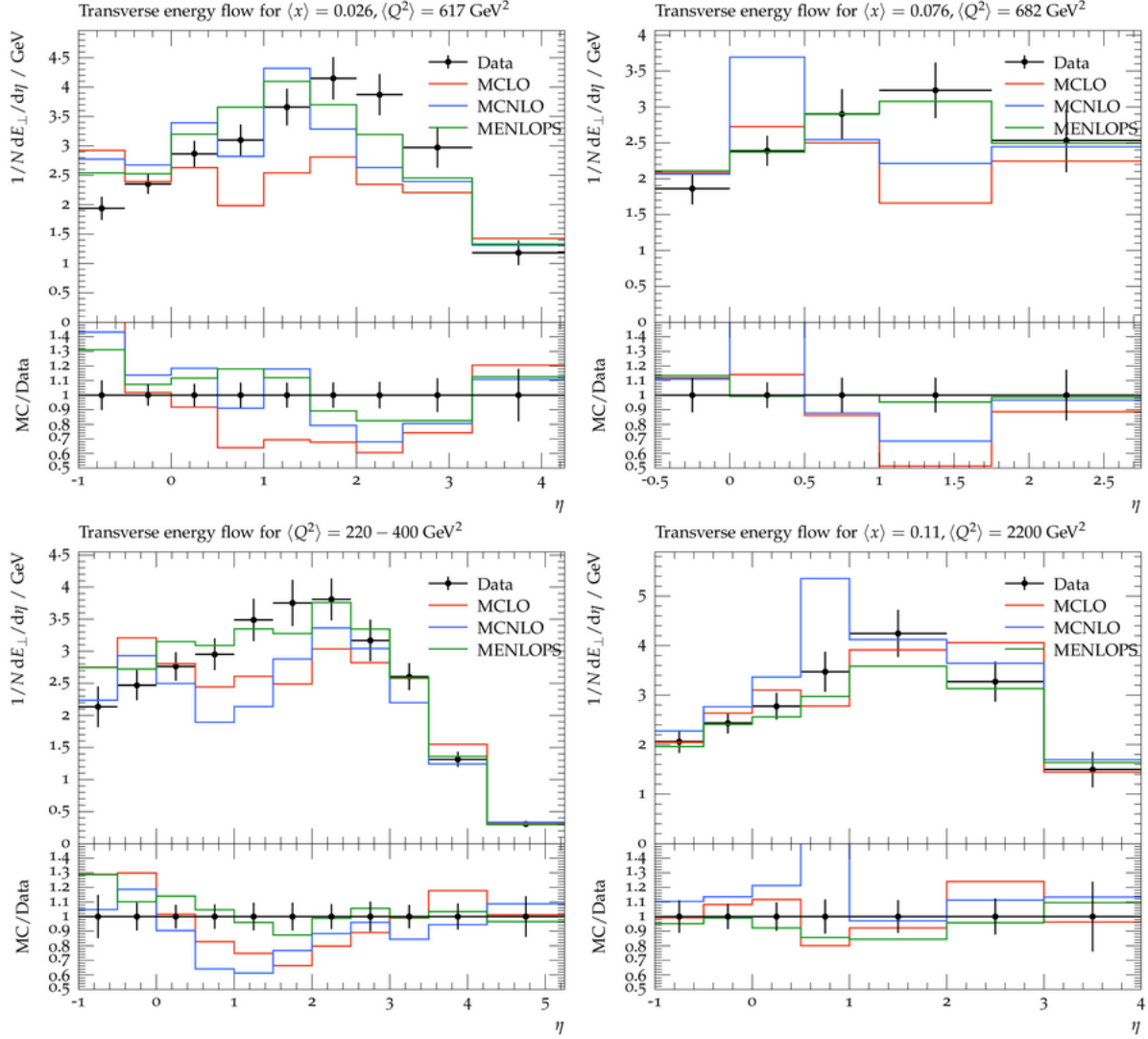


Figure 7: Sherpa2, 1M events, Beam energies-  $p = 820 \text{ GeV}^2, e = 27.5 \text{ GeV}^2$ . **High  $Q^2$  region.** The large variations between MC and HERA data can be attributed to weak interaction processes, occurring for  $Q^2$  greater than  $100 \text{ GeV}^2$

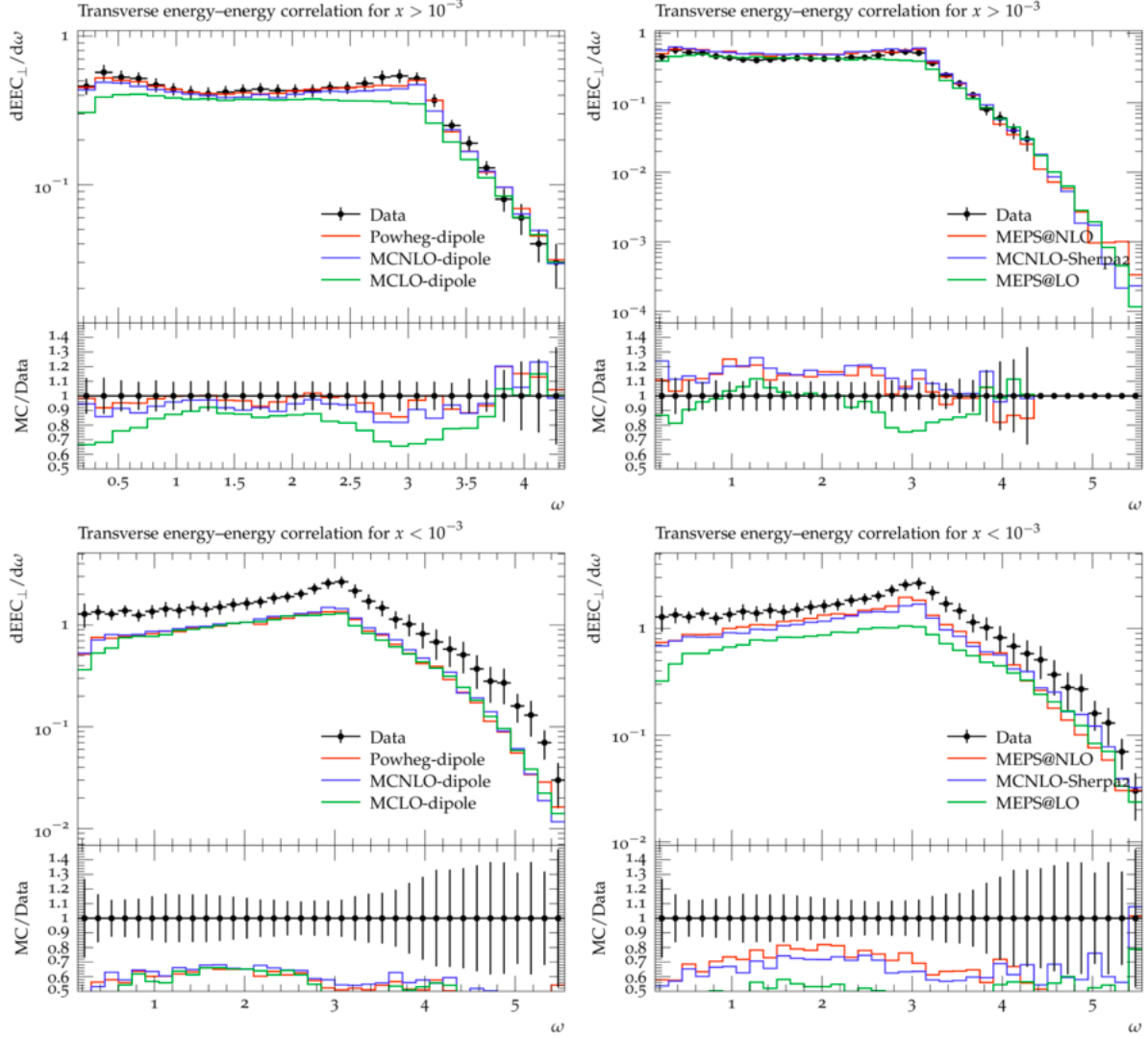


Figure 8: column1 : Herwig7, column2 : Sherpa2 MC generators, 10K events, at beam energy of  $p = 820 \text{ GeV}^2$ ,  $e = 26.7 \text{ GeV}^2$ . **Low X-regime** is the least explored, and there are opportunities to test some extreme QCD effects here. QCD effects owing to high parton densities are expected this region. Its a region of gluon-saturation, wherein the parton wavefunctions start overlapping in phase-space, and the number of partons created depends non-linearly on the number of previous partons. Pertaining to this reasons, the MC data of transverse energy correlations plots deviate from HERA data in low x region.

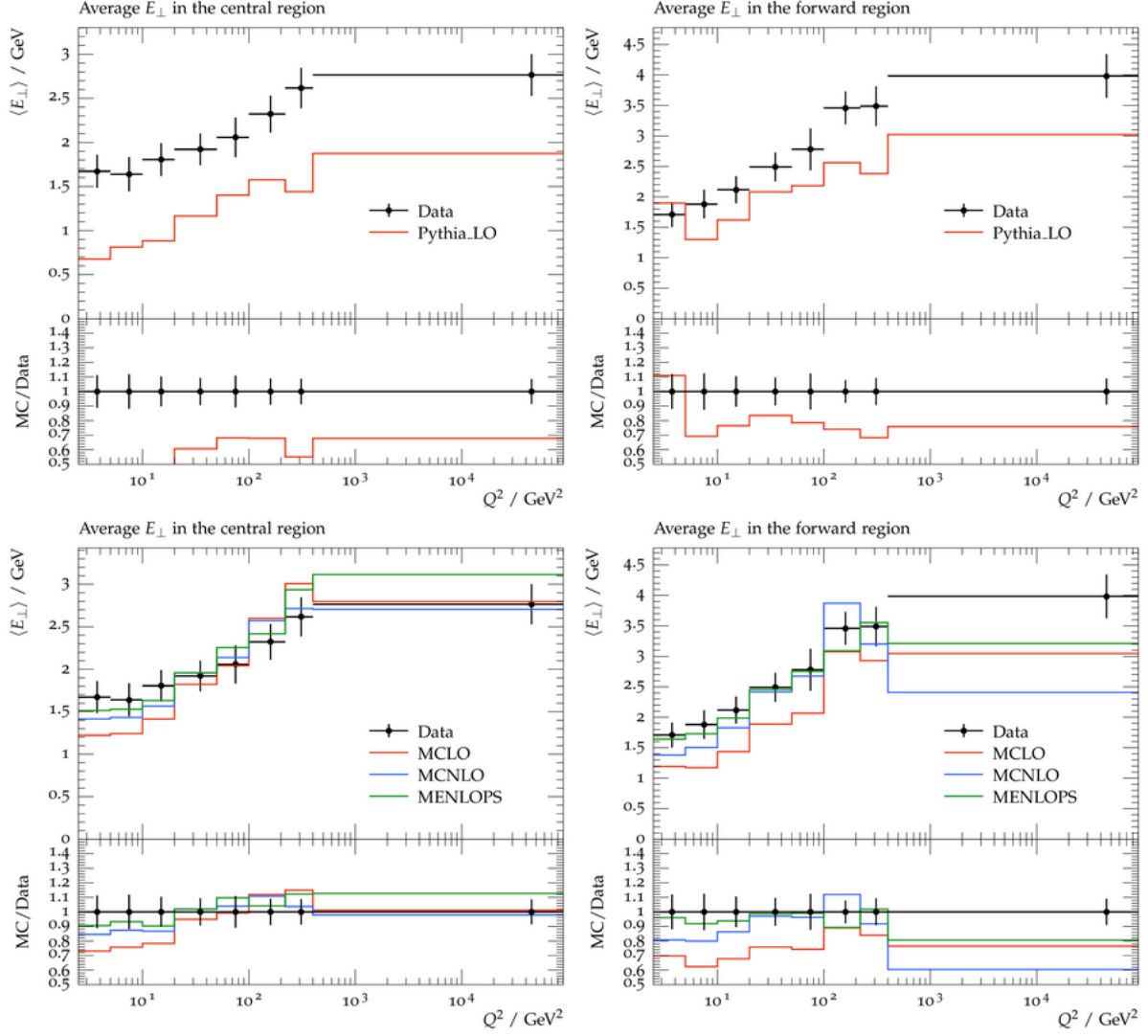


Figure 9: Pythia8 and Sherpa2, 1M events, Beam energies-  $p = 820\text{GeV}^2$ ,  $e = 27.5\text{GeV}^2$ . Central regions corresponds to  $\eta < 0.5$  and Forward region is for  $2 > \eta > 2$ . Variations in Pythia MC are maximum. Both the MCs fail to explain average  $E_T$  distribution in higher  $Q^2$  region.



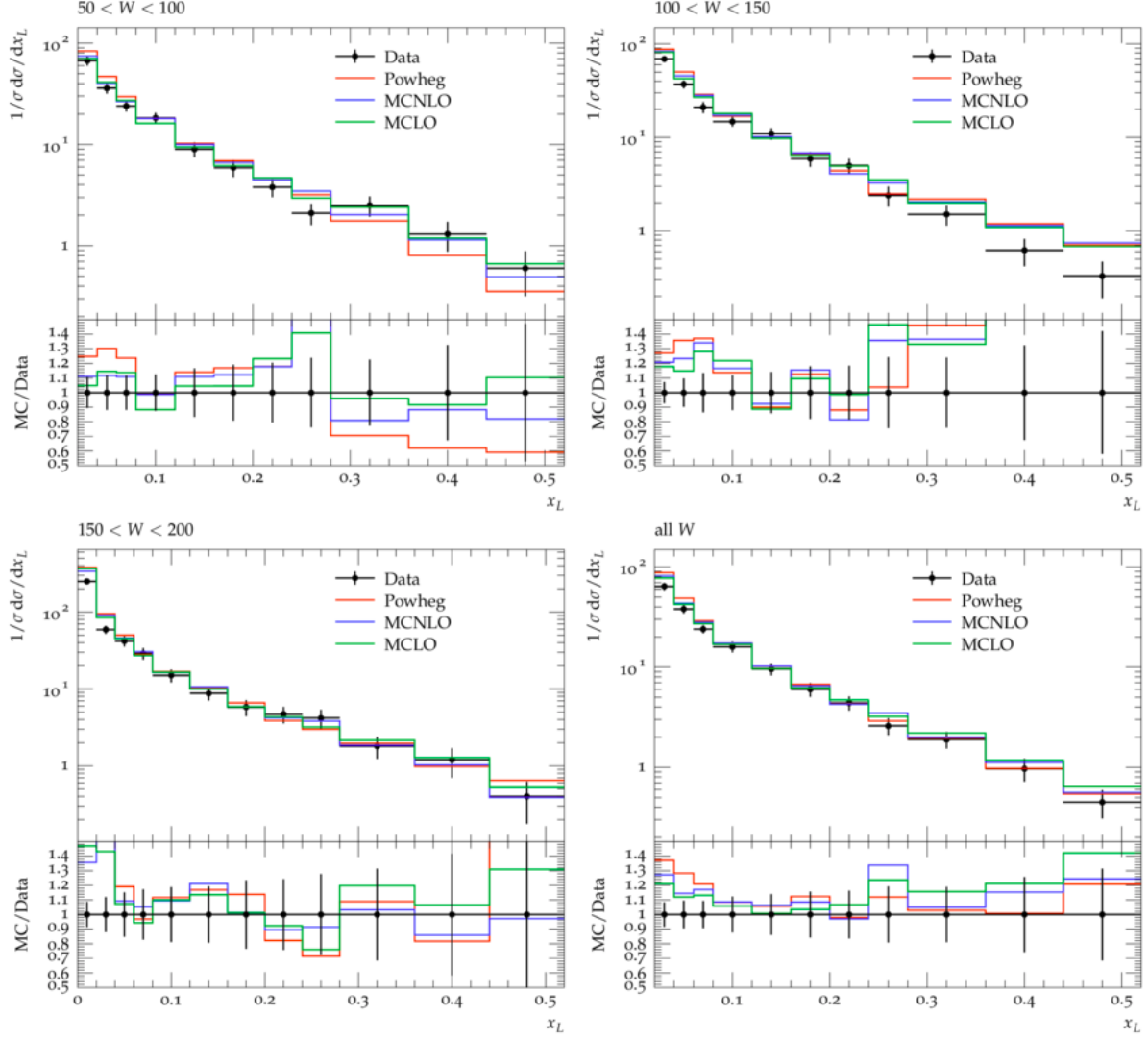


Figure 10: Herwig7, 100K events, Beam energies-  $p = 820\text{GeV}^2$ ,  $e = 26.7\text{GeV}^2$ . Scaled charged particle spectra in different  $W$  ranges. All MC models fit the data quite well in lower  $x_L$  regions. The causes of deviations in high  $x_L$  region needs to be explored

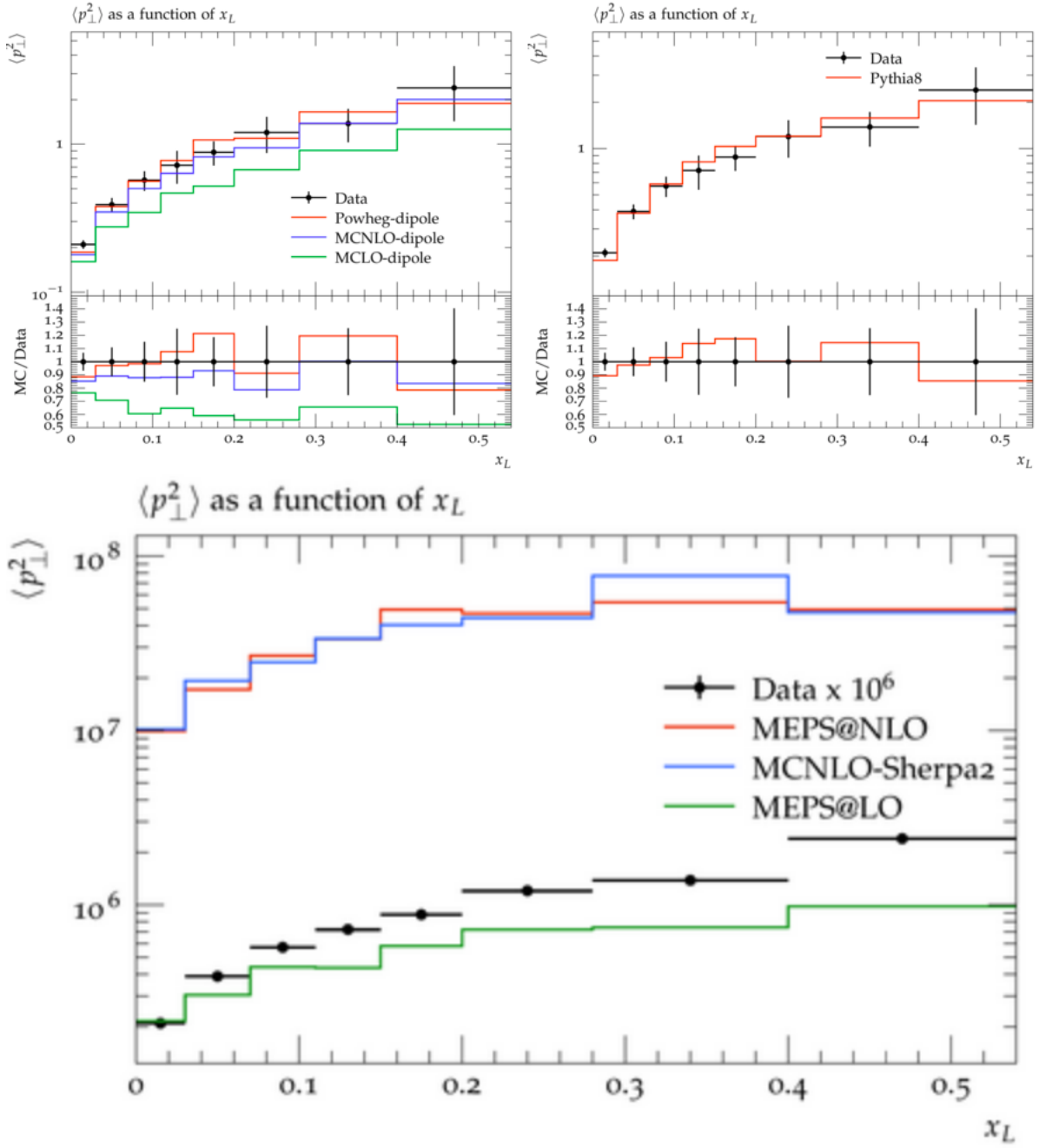


Figure 11: Herwig7, Pythia8, Sherpa (respectively) MC generators, 100K events, at beam energy of  $p = 820 \text{ GeV}^2$ ,  $e = 26.7 \text{ GeV}^2$ . The wide deviation in Sherpa MC data by an order of magnitude of  $10^5$  is the most noticeable and change in MC-tunings is required.

## 5 Charged particle Multiplicity Distributions in DIS at HERA energies

The study of the hadronization and the parton fragmentation process in Deep Inelastic Scatterings can be studied by the inclusive charged particle multiplicity distributions. It is one of the basic global observable which is measured to characterise the final state. The probability distribution of the number of charged hadrons produced in a given region of phase space is known as the multiplicity distribution. The fluctuations in multiplicity are a direct measure of the strength of correlations among the produced hadrons. In high energy physics, the particle correlations have been extensively used as probes of the hadronization dynamics. The particle correlations is explored by studying the various moments and cumulants of order  $q$  of the multiplicity distribution in a given phase space.

### 5.1 Analysis

The charged particle multiplicity analysis was carried out by obtaining the distributions using Pythia8 and Herwig7 event generators and comparing them with the available data at HERA energies. The Figure 1, 2,3 and 4 shows the multiplicity distributions obtained for different regions of  $W$  in different pseudo-rapidity intervals.

### 5.2 Kinematic selection

As mentioned earlier, the data used for the comparison was taken during the running period of 1994 of the HERA storage ring at DESY. The Centre of Mass collision energy of the system was 300 GeV with respective energies of the positrons and protons used for collision being 27.5 GeV and 820 GeV. The phase space was also selected in such a way to minimize the all other undesired effects.

The the energy of the scattered electron/positron was required to be  $e' > 12$  GeV to select the neutral current DIS events. This also helps to reduce the photoproduction background to less than 1%. Rapidity-gap events are removed from the data sample by requiring that the total energy deposited between polar angles  $4.4 < \theta < 15$  should be less than 0.5 GeV. Only those tracks which lie between the range  $15 < \theta < 155$  for the polar angle are selected. The pseudorapidity, in the hadronic centre of mass frame, range for the for the experiment was taken in the  $\eta^* > 0$  or the so-called full current hemisphere and for the range  $1 < \eta^* < 3$ . These domains were later separated into more finer regions. The main observables apart from charged multiplicity are the mean charged multiplicity  $\langle n \rangle$ , the generalised dispersions,  $D_q = \left[ \overline{(n - \bar{n})^q} \right]^{1/q}$  and the normalised multiplicity moments,  $C_q = \langle n^q \rangle / \langle n \rangle^q$ . The virtuality cuts applied were in the range  $10 < Q^2 < 1000$ . The invariant mass squared of the hadronic system was required to be  $80 < W < 220$  GeV.

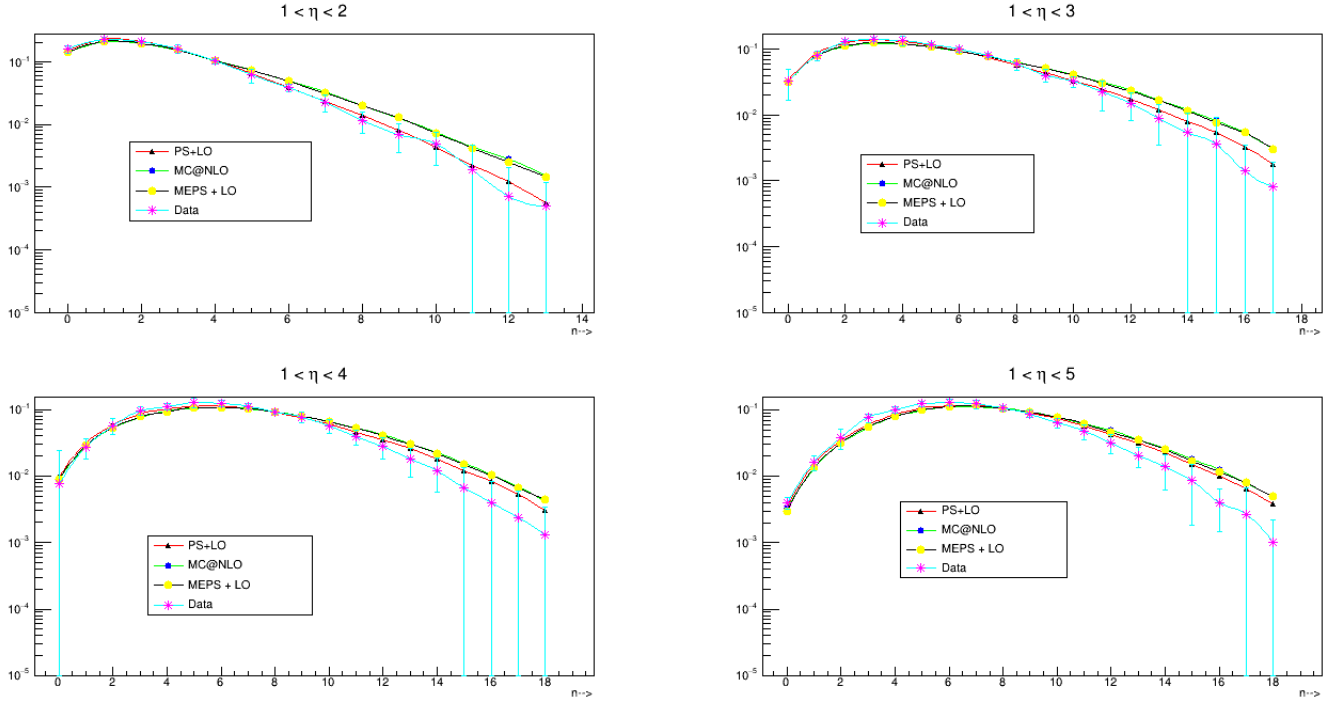


Figure 12: The multiplicity distribution has been measured, in the kinematic regions in  $W$  and  $Q^2$  shown in the following figures, for charged particles with pseudorapidity in the domains  $1 \leq \eta \leq \eta_c$  with  $\eta_c = 2, 3, 4, 5$  and in intervals of unit pseudorapidity centered at  $\eta = 2.5, 3.5, 4.5$ , as well as for the full current hemisphere defined as the domain  $\eta > 0$ . Here, Charged Particle Multiplicity distribution for  $80\text{GeV} < W < 115\text{GeV}$

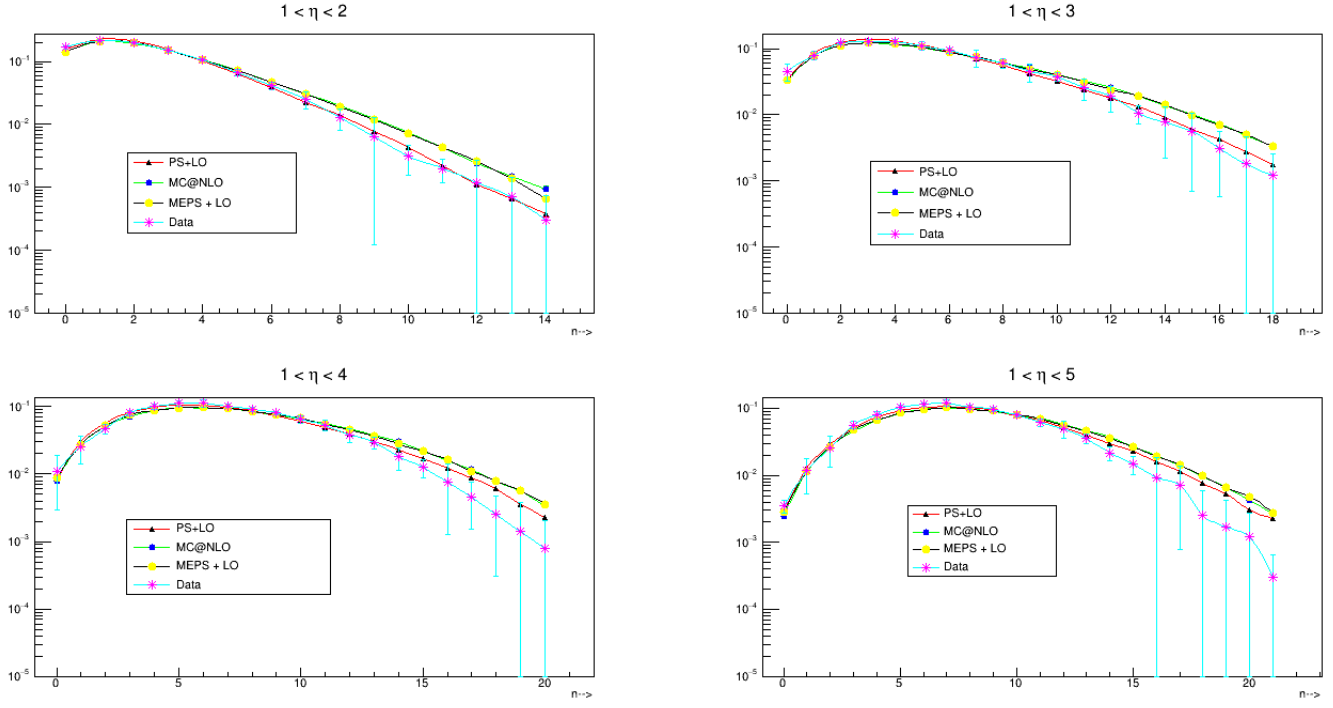


Figure 13: Charged Particle Multiplicity distribution for  $115 \text{ GeV} < W < 150 \text{ GeV}$

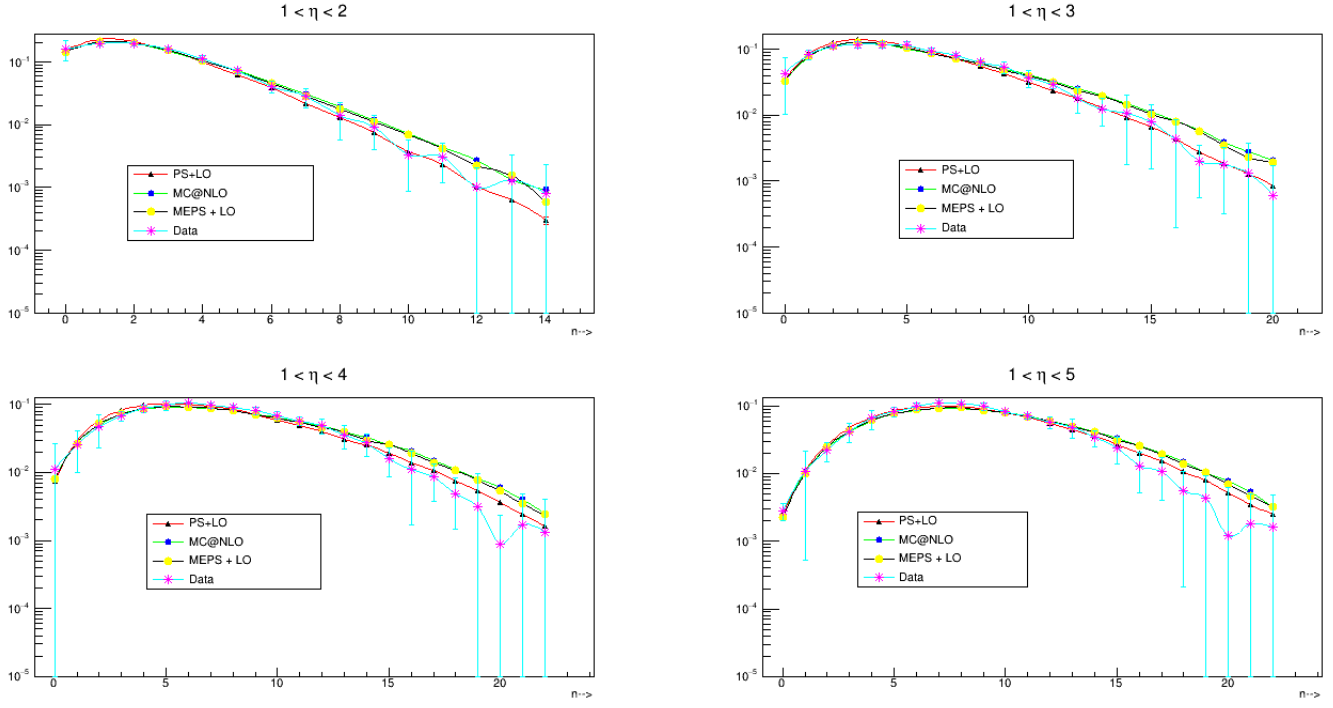


Figure 14: Charged Particle Multiplicity distribution for  $150 \text{ GeV} < W < 185 \text{ GeV}$

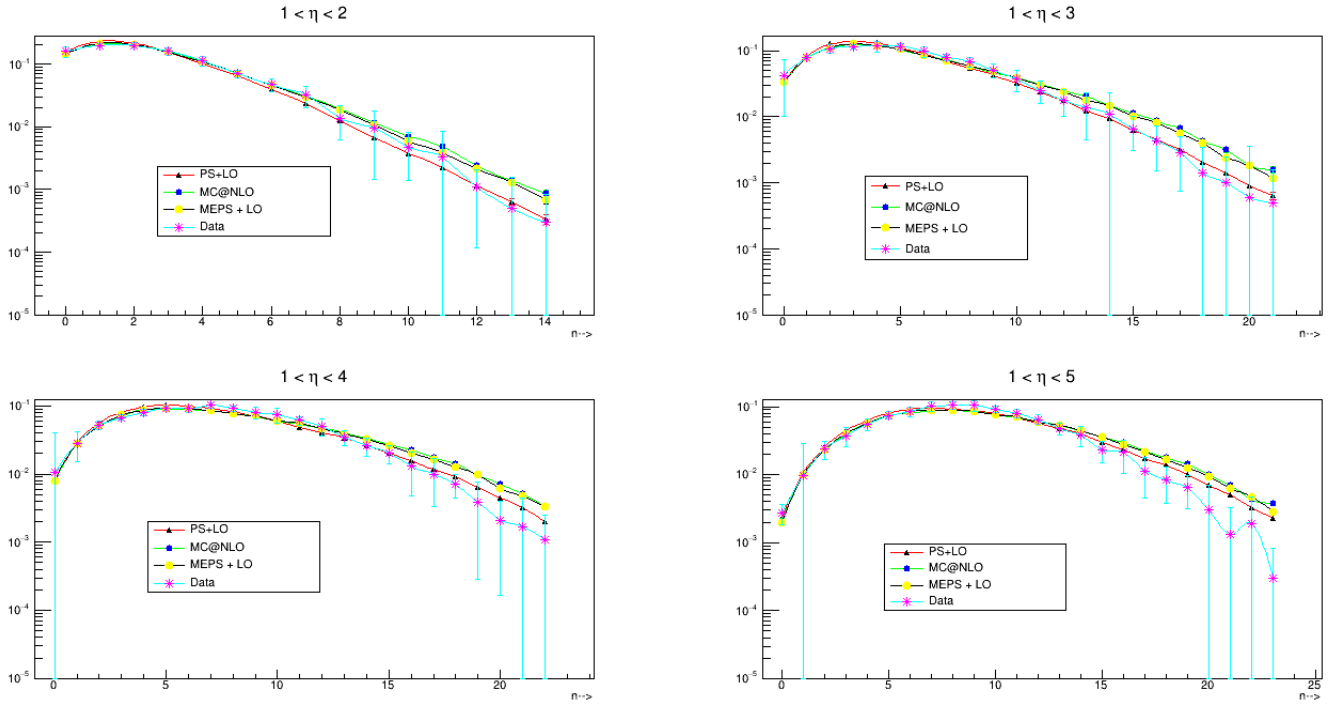


Figure 15: Charged Particle Multiplicity distribution for  $185\text{GeV} < W < 220\text{GeV}$

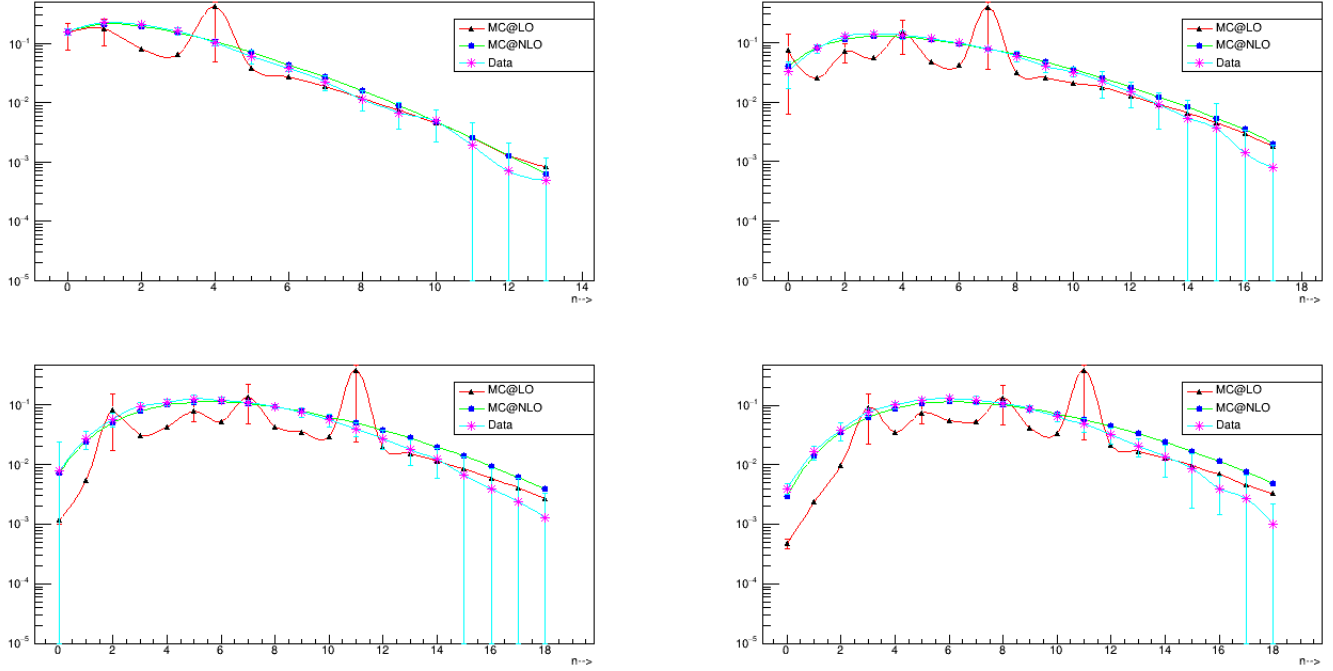


Figure 16: Charged Particle Multiplicity distribution for  $80 \text{ GeV} < W < 115 \text{ GeV}$



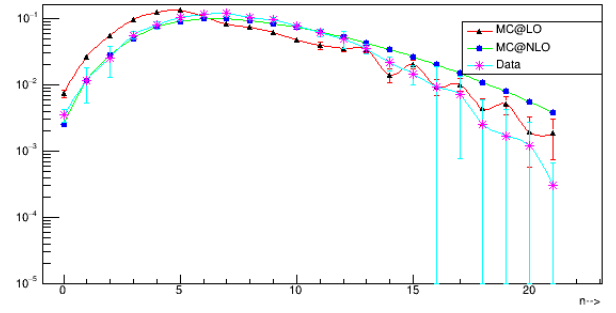
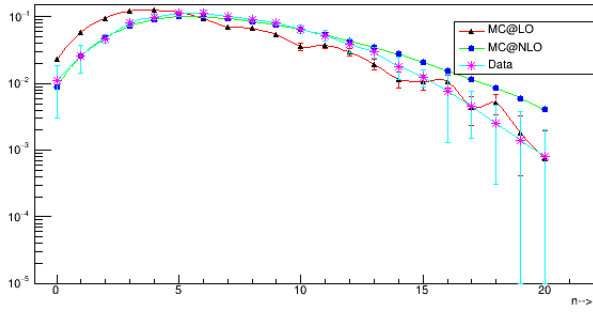
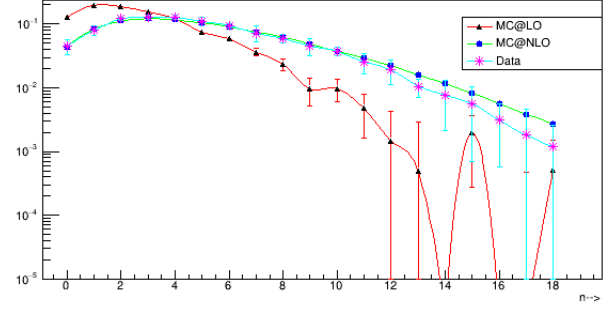
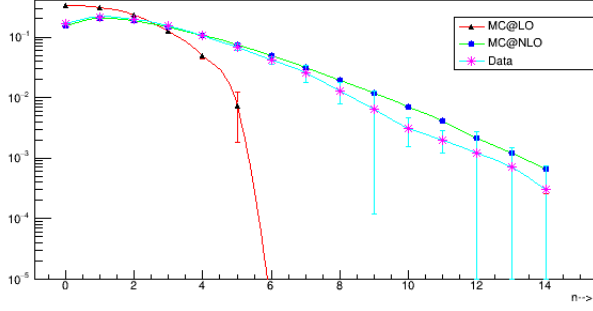


Figure 17: Charged Particle Multiplicity distribution for  $115\text{GeV} < W < 150\text{GeV}$

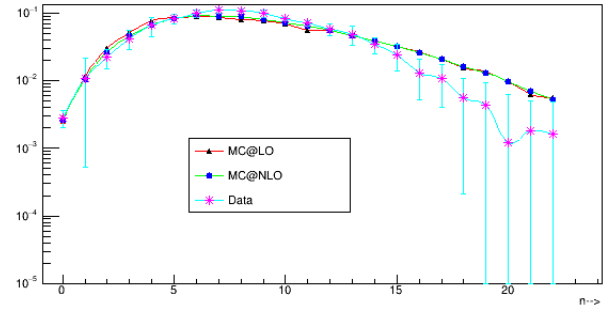
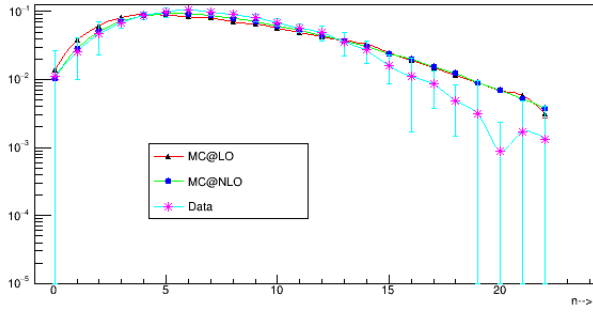
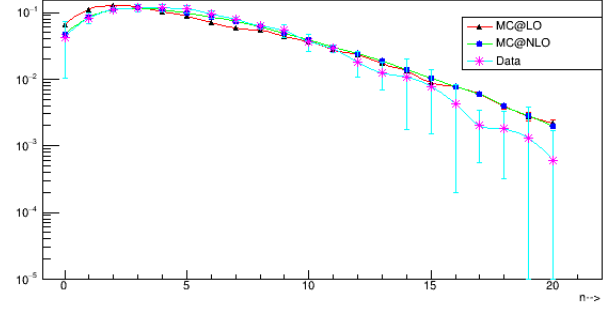
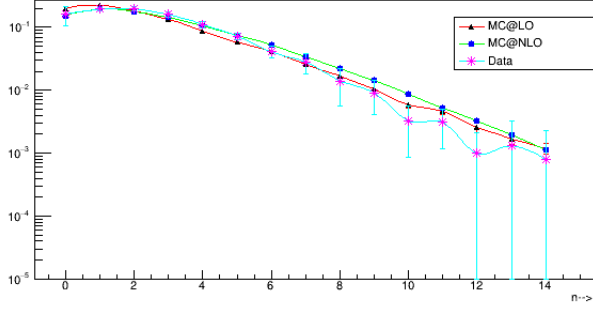


Figure 18: Charged Particle Multiplicity distribution for  $150\text{GeV} < W < 185\text{GeV}$

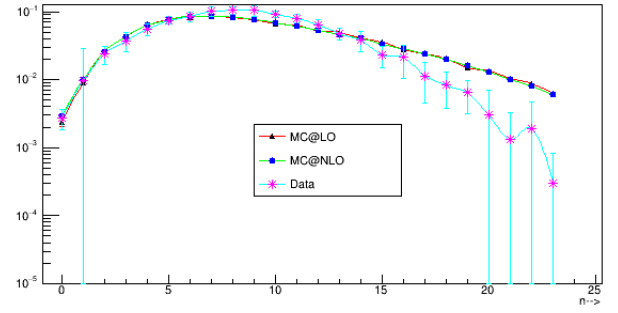
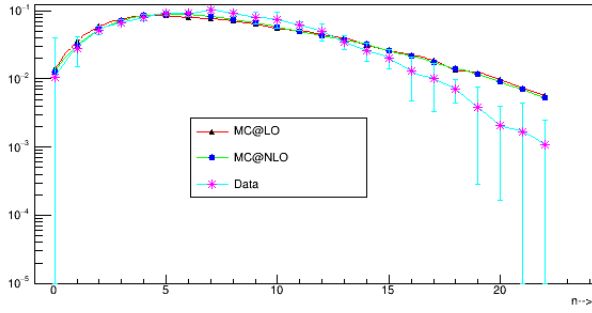
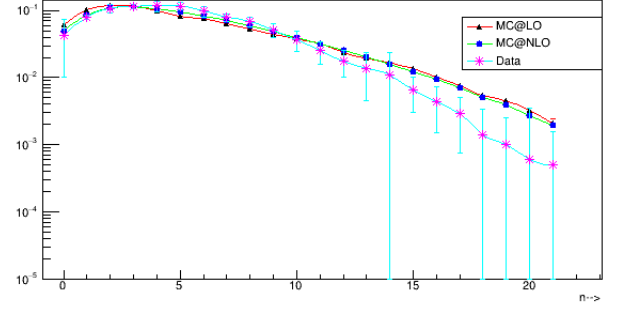
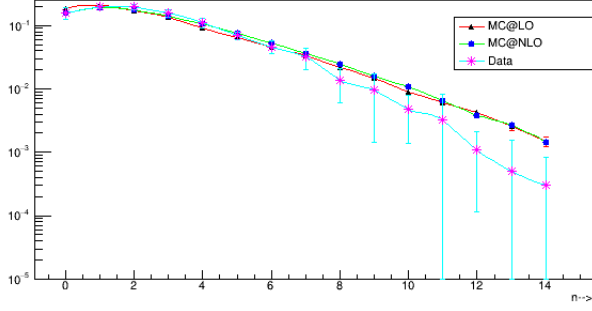
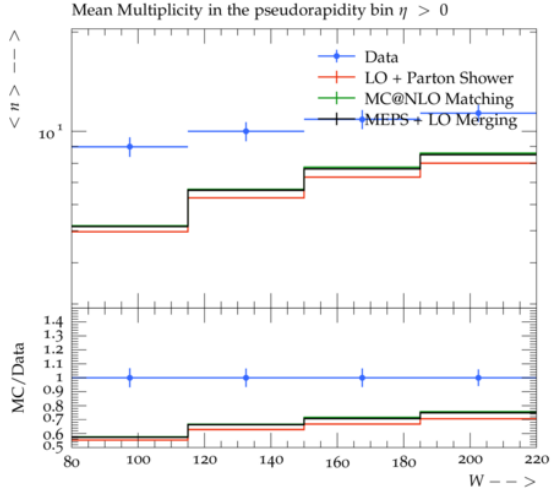
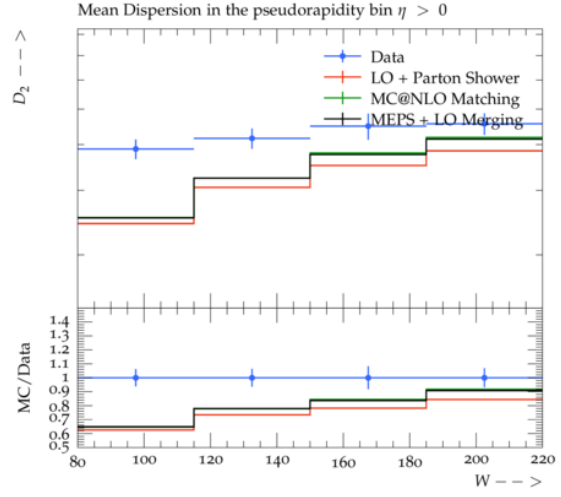


Figure 19: Charged Particle Multiplicity distribution for  $185\text{GeV} < W < 220\text{GeV}$

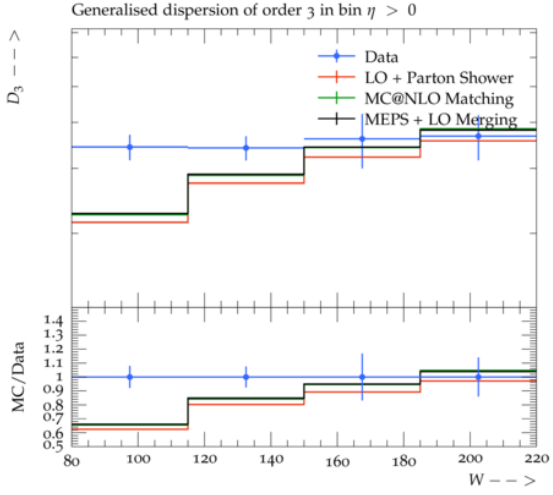




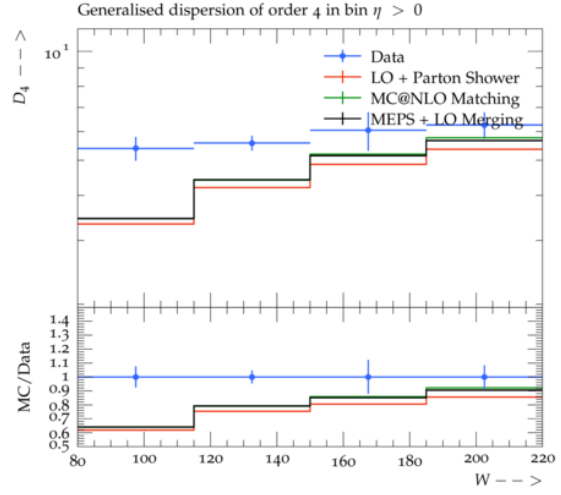
(a)



(b)



(c)



(d)

Figure 20: Mean Multiplicity,  $\langle n \rangle$ ,  $D_i$ ,  $C_i = \langle n^i \rangle / \langle n \rangle^i$  as a function of  $W$  for different  $\eta$  bins,  $\langle n \rangle$

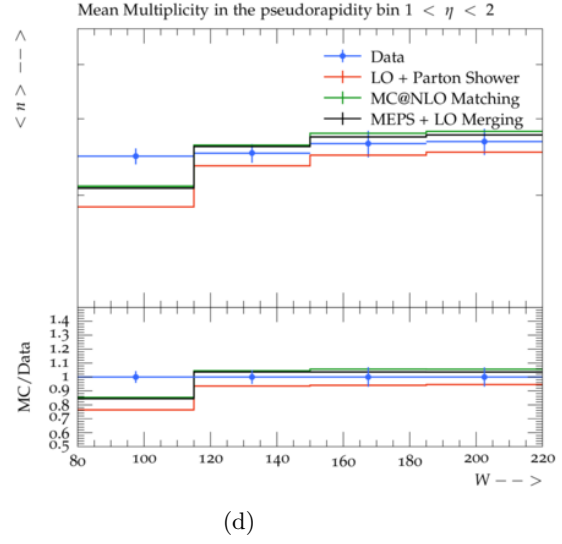
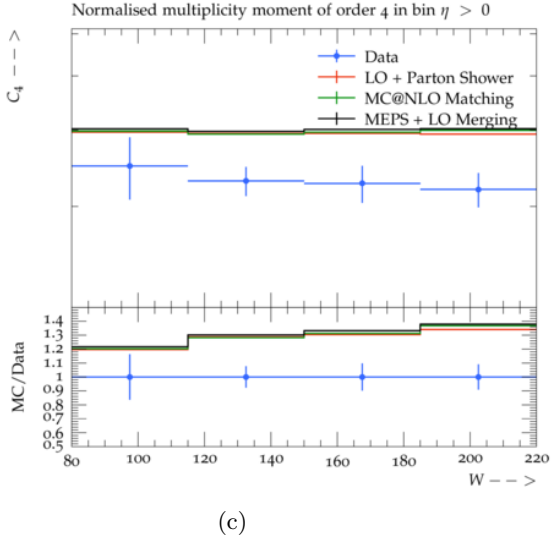
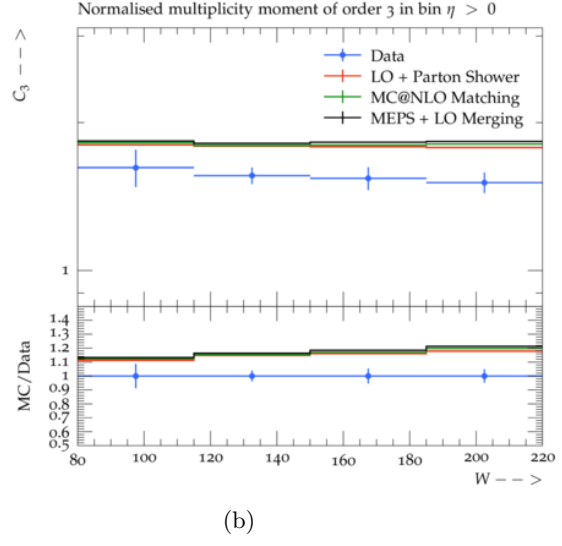
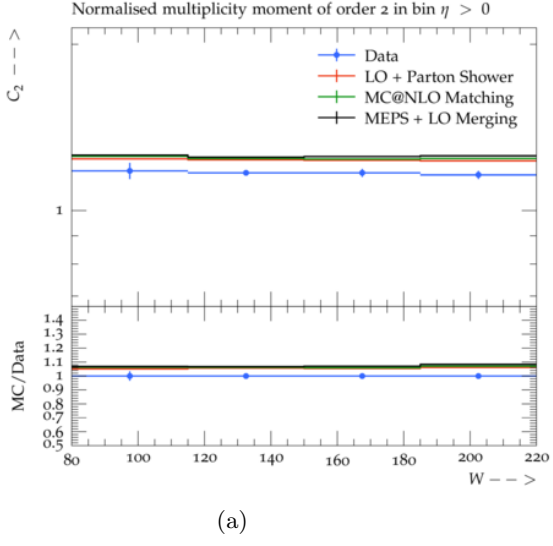


Figure 21: The inclusive sections as a function of  $x$  for two  $Q^2$  intervals, (  $35 < Q^2 < 100 \text{ GeV}^2$  ) and (  $10 < Q^2 < 35 \text{ GeV}^2$  ).

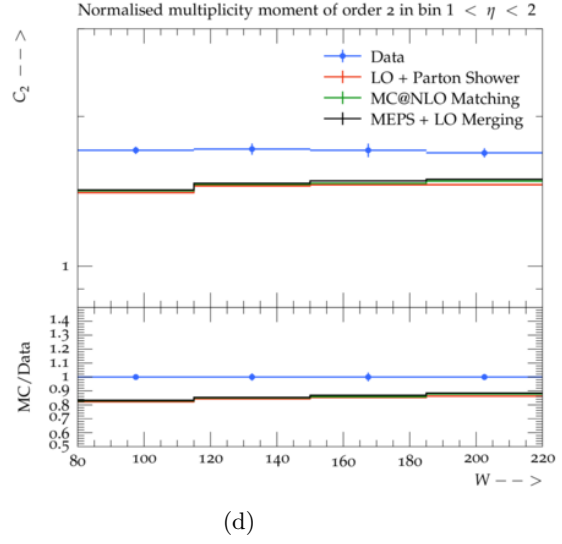
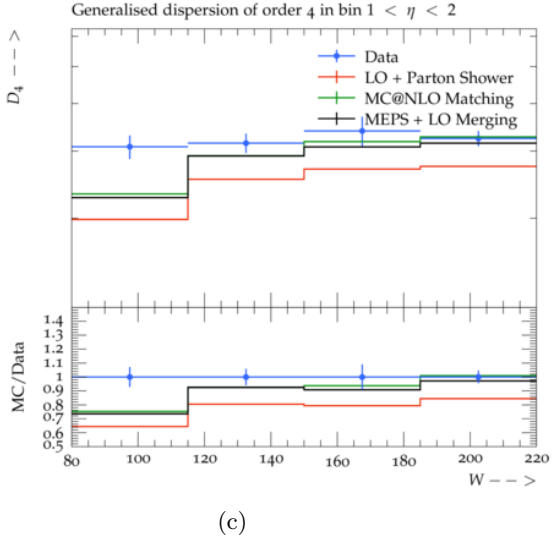
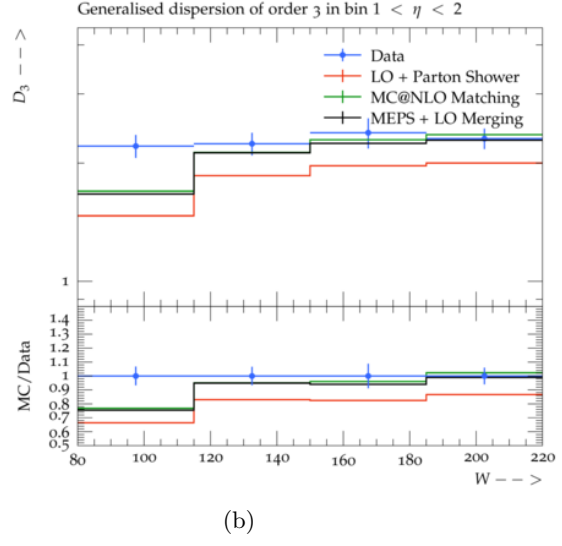
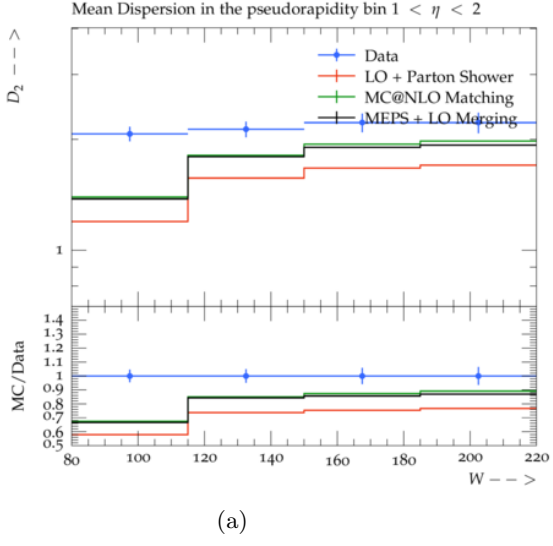


Figure 22: The inclusive sections as a function of  $x$  for two  $Q^2$  intervals, ( $35 < Q^2 < 100 \text{ GeV}^2$ ) and ( $10 < Q^2 < 35 \text{ GeV}^2$ ).





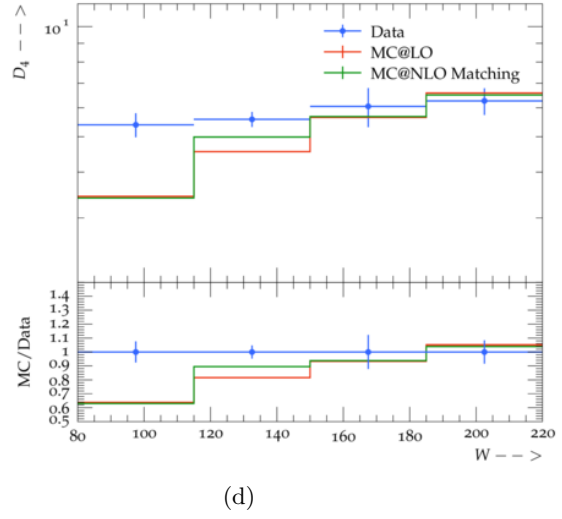
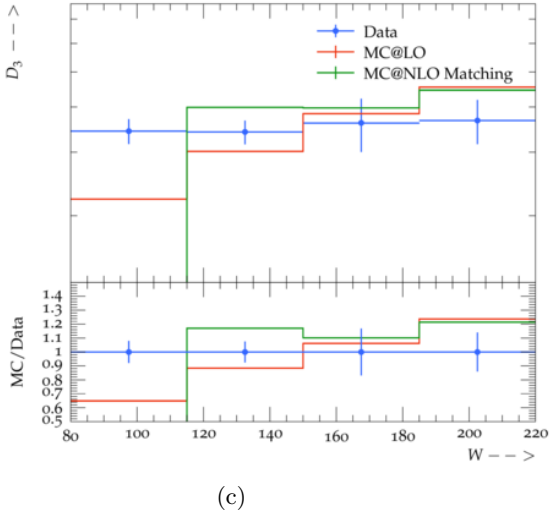
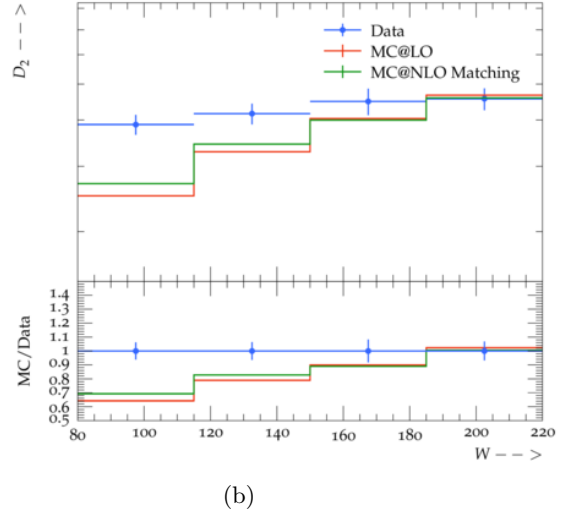
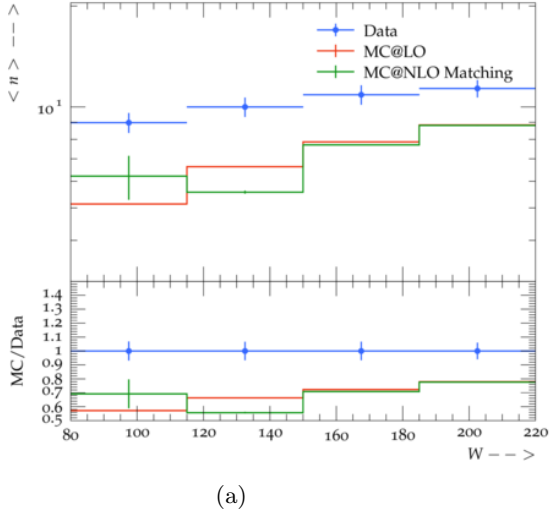
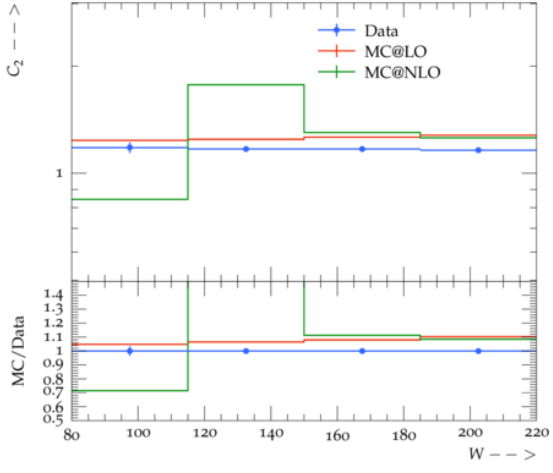
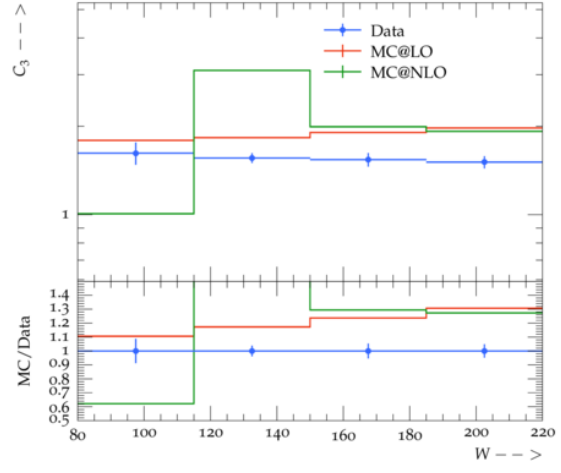


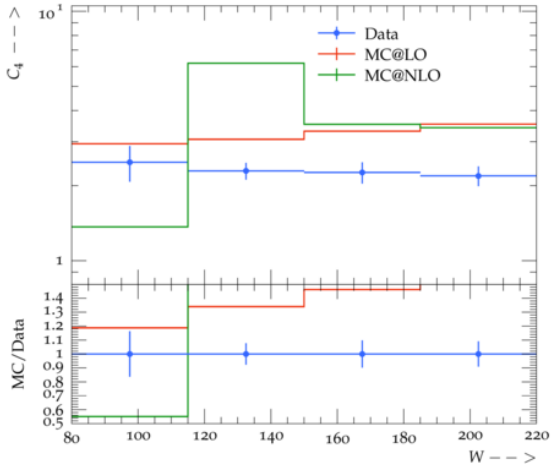
Figure 23: Mean Multiplicity,  $\langle n \rangle$ ,  $D_i$ ,  $C_i = \langle n^i \rangle / \langle n \rangle^i$  as a function of  $W$  for different  $\eta$  bins,  $\langle n \rangle$



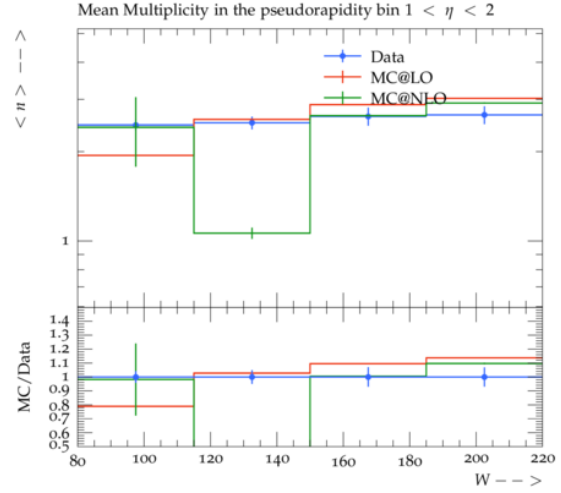
(a)



(b)



(c)



(d)

Figure 24: The inclusive sections as a function of  $x$  for two  $Q^2$  intervals, ( $35 < Q^2 < 100 \text{ GeV}^2$ ) and ( $10 < Q^2 < 35 \text{ GeV}^2$ ).

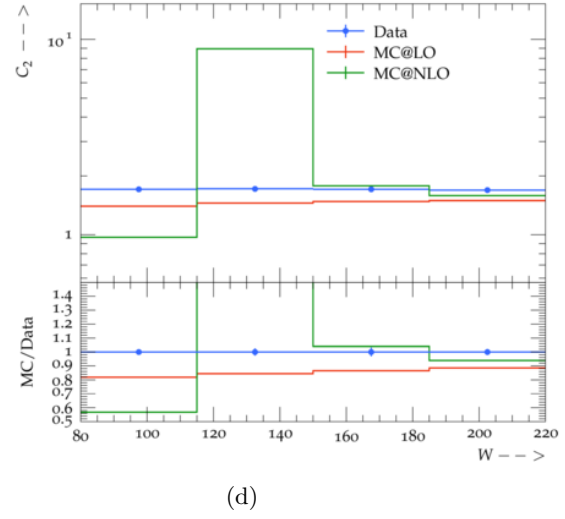
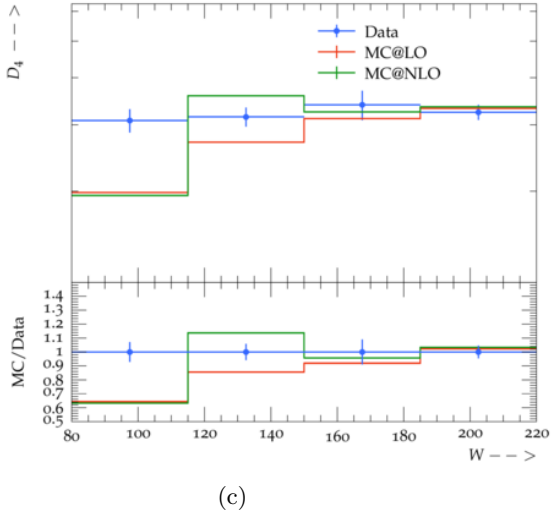
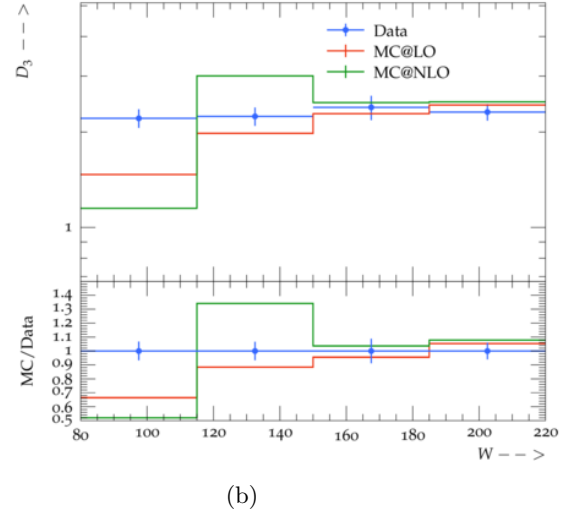
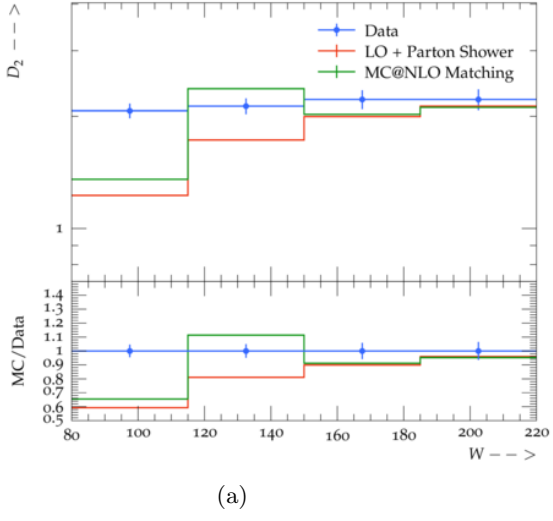


Figure 25: The inclusive sections as a function of  $x$  for two  $Q^2$  intervals, ( $35 < Q^2 < 100 \text{ GeV}^2$ ) and ( $10 < Q^2 < 35 \text{ GeV}^2$ ).

## 6 $D^*$ production cross-section

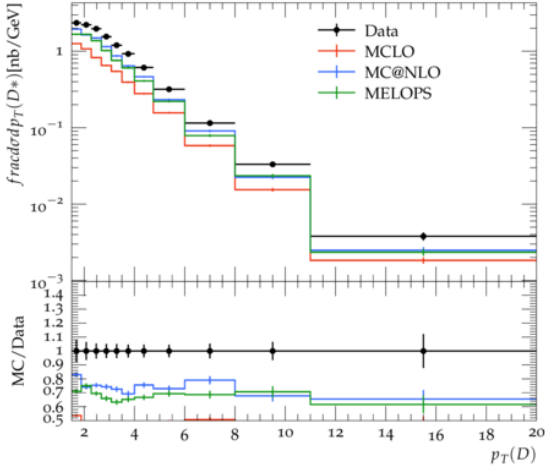
The motivation for this data comparison comes from the importance of information available from the charm production measurements for testing quantum chromodynamics (QCD). This is because the main process by which charm quarks are produced involves boson gluon fusion process,  $\rightarrow cc$  which in turn depends on the gluon distribution inside the proton. The data taken for the analysis comes from the HERA running periods (1992-2000) and (2003-2007). It also provided useful information in terms of the charm quark mass  $m_c$ , improving the predictions for the cross-section of  $Z$ - and  $W$ - production. The data was extrapolated to full phase space for comparison purposes but to minimise dependence theoretical input, the comparison was properly done directly in the visible phase space region with respect to cuts on inclusive DIS variables like the photon virtuality and inelasticity,  $y$ . The data also provides a good signal-to-background ratio with small uncertainties.

### 6.1 Kinematic selection

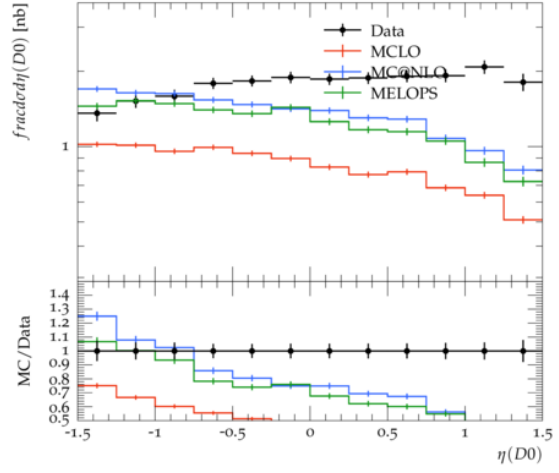
The centre-of-mass energy of the data sample is  $\sqrt{s} = 318$  GeV. The data corresponds to single differential cross-section for  $D^* \pm$  production with respect to the kinematic variables, transverse momentum,  $p_T(D^*)$ , pseudorapidity,  $\eta(D^*)$  and the elasticity,  $z(D^*) = (E(D^*) - p_z(D^*))/(2E)$  both measured in the lab frame and global variables  $Q^2$  and  $y$ .

Table 1: Phase space selection

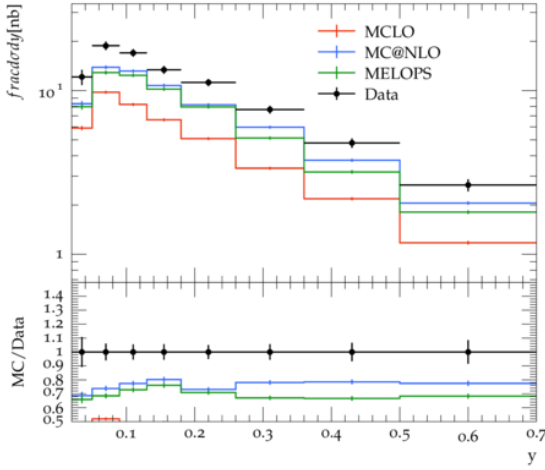
Range in	Single differential cross-section
$Q^2$ ( $GeV^2$ )	10-1000
$y$	0.02 - 0.7
$p_T(D^*)(GeV)$	$>1.5$
$ \eta(D^*) $	$<1.5$



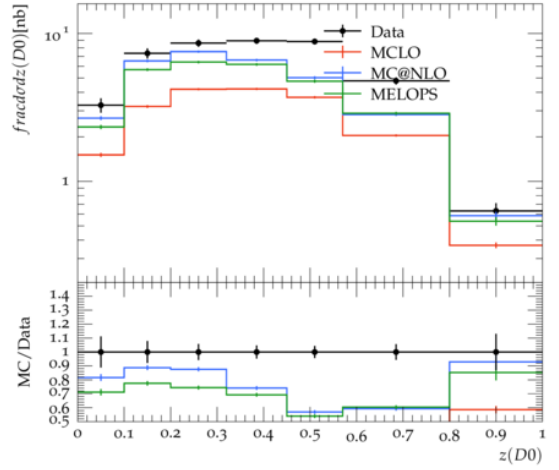
(a)



(b)



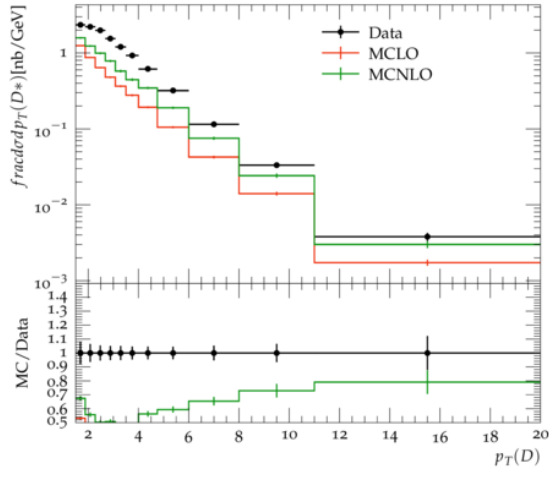
(c)



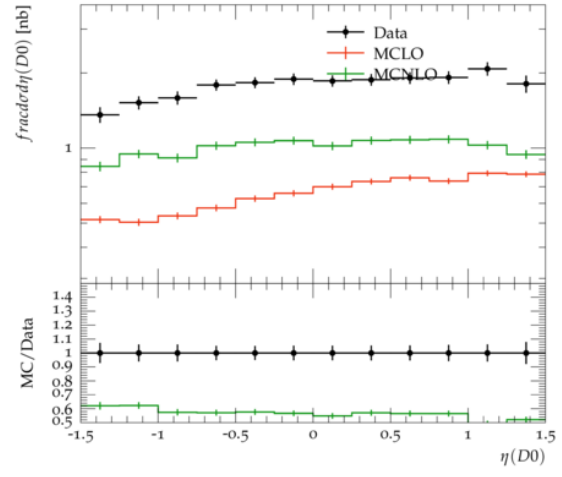
(d)

Figure 26: The data corresponds to single differential cross-section for  $D^*\pm$  production with respect to the kinematic variables, transverse momentum,  $p_T(D^*)$ , pseudorapidity,  $\eta(D^*)$  and the elasticity,  $z(D^*) = (E(D^*) - p_z(D^*))/(2E)$  both measured in the lab frame and global variables  $Q^2$  and  $y$ . Here we have ones from Sherpa 2.2.10

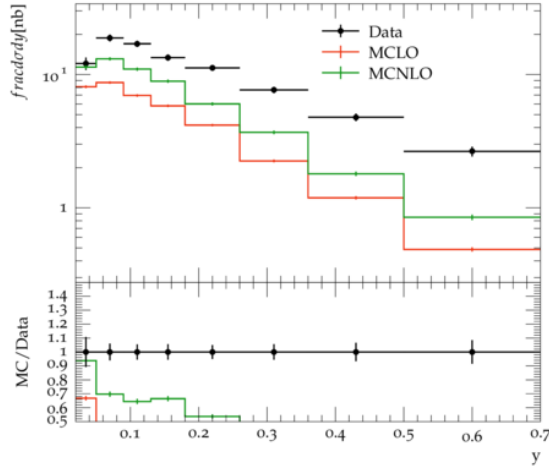




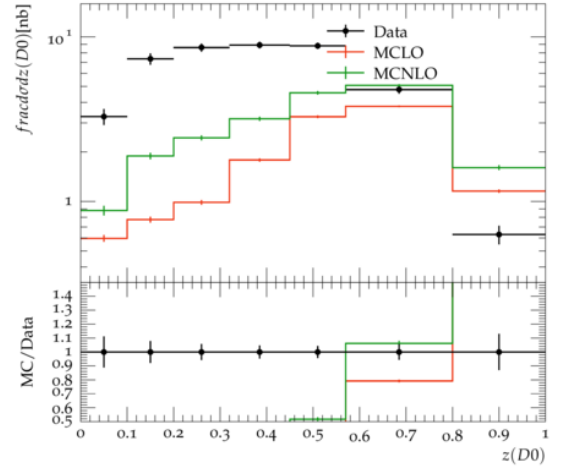
(a)



(b)



(c)



(d)

Figure 27: This is from Herwig 7.2.1

## 7 Event Shape variables

The event shape variables data has been compared with those available from H1 collaboration as well as the ZEUS collaboration[36]. Similar to all the previous experiments, the hadronic final states produced in  $ep$  collisions through the neutral current channel offer an opportunity to understand hadronisation process as well as measuring the strong coupling constant for a wide range of virtuality  $Q^2$ . Event shape variables in DIS can be used for studying the coupling constant for the strong force provided that it is possible to separate the particles can be divided into the current fragmentation region produced from the struck quark and the target fragmentation region produced from the proton remnant. As was specified in one of the experiments earlier, the Breit frame is a useful frame of reference where there is minimal contamination of the current region from the target region. Also, in this reference frame, we work with a purely space-like photon with momenta  $q_\gamma = 0, 0, 0, -Q$  which collides with a quark carrying longitudinal momentum  $p_{qz} = Q/2$ . The struck quark is scattered back into the current region or hemisphere with longitudinal momentum  $p_{qz} = -Q/2$  whereas the proton remnant undergoes fragmentation in the opposite hemisphere also called the target region. This obviously implies that the energy for fragmentation available in the current hemisphere is  $Q/2$  and it also makes comparison with collision data involving  $e^+e^-$  easier.

For the data validation purposes, certain event shape variables are considered in current region of Breit frame which are namely, Thrust, Jet Broadening and Jet mass.

### 7.0.1 Kinematic selection

The data used for the comparison comes from both the H1 detector and ZEUS detector at HERA for the running period 1994-1996. with a centre-of-mass energy of 300 GeV. The kinematic range of the phase space region used for data collection are as follows. The virtuality of the collision was restricted to the range  $7 < Q < 100$  GeV. The energy of the scattered lepton, here electron has to be greater than ,  $E_e > 10$  GeV. The polar angle of the scattered lepton should lie between the angular range  $157 < \theta_e < 173$  for the low Q sample and between  $30 < \theta_e < 150$ . The energy in the forward region should be  $E > 0.5$  GeV, whereas by the forward region it is meant that the polar angular range  $4 < \theta_h < 15$ . This is to eliminate the diffractive events as well as the ones with large rapidity gaps. Finally, the energy in the Breit frame is required to be greater than  $0.1 Q$ . Now, that the phase space selection is completed, its proper to look at the equations for the event shape variables under consideration. The event shape variables that are infrared safe namely, Thrust which is basically the measurement of the collimation of the longitudinal component of a hadronic system and Jet Broadening which is the transverse or the complimentary aspect of what is represented by Thrust. In its most general for, thrust and broadening can be defined by the following equations,

$$T = \frac{\sum_i |p_i \cdot n|}{\sum_i |p_i|}$$

for thrust and

$$B = \frac{\sum_i |p_i \times n|}{\sum_i |p_i|}$$

where the sum runs over all the final state hadrons and  $p_i$  is the momentum of that final state particle. For the purpose of data validation the event shape variables are



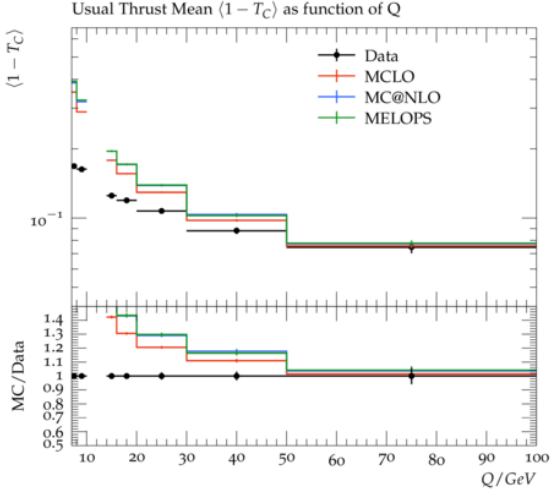
considered with respect to particular axis are:

$$T_c = \max \frac{\Sigma_h |\mathbf{p}_h \cdot \mathbf{n}_T|}{\Sigma_h |\mathbf{p}_h|}$$

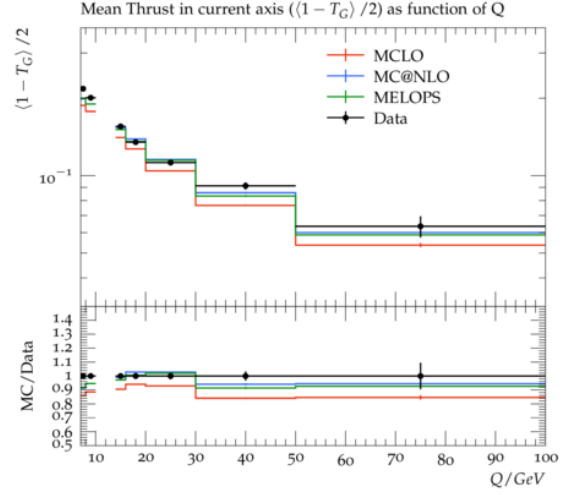
where the axis in consideration is the thrust axis which is the any direction,  $\mathbf{n}_T$  that maximises the thrust value.

$$T_z = \frac{\Sigma_h |\mathbf{p}_h \cdot \mathbf{n}|}{\Sigma_h |\mathbf{p}_h|} = \frac{\Sigma_h |\mathbf{p}_{zh}|}{\Sigma_h |\mathbf{p}_h|}$$

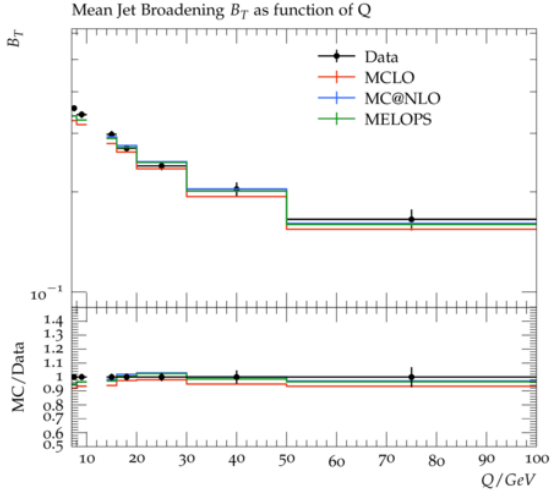
where the measurement is with respect to the current hemisphere axis which is  $\mathbf{n}$  is 0,0,-1 and is in the same direction as the virtual boson direction.



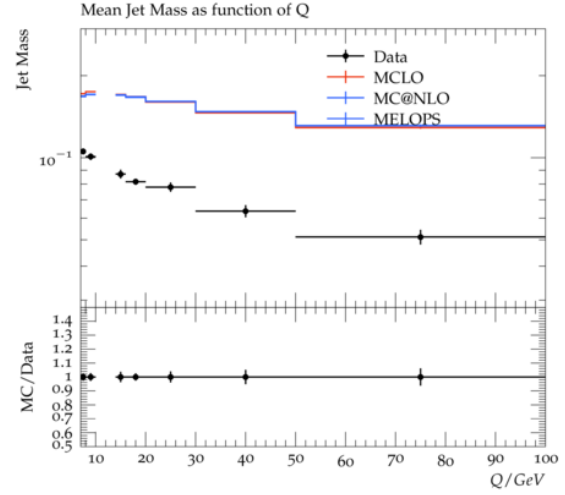
(a)



(b)



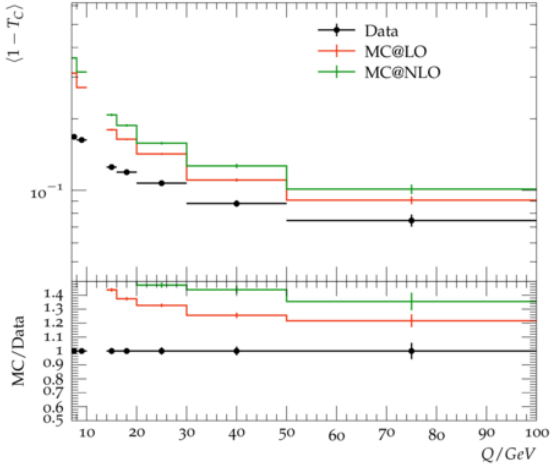
(c)



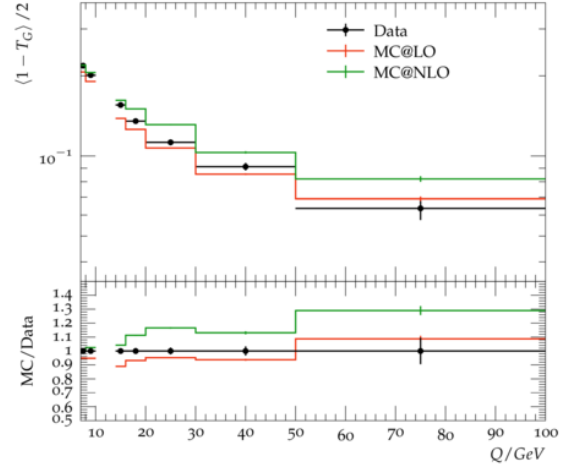
(d)

Figure 28: The mean value of  $\langle 1 - T_C \rangle$  where thrust is the usual definition, similarly for jet broadening  $B_T$ , as well as with the axis of thrust taken with respect to the virtual photon direction. The kinematics cuts are for the ranges (7,100) in  $Q/GeV$  and ( 0.05, 0.8) in elasticity.

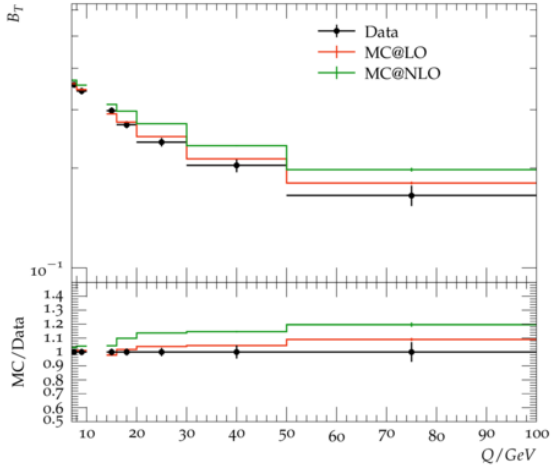




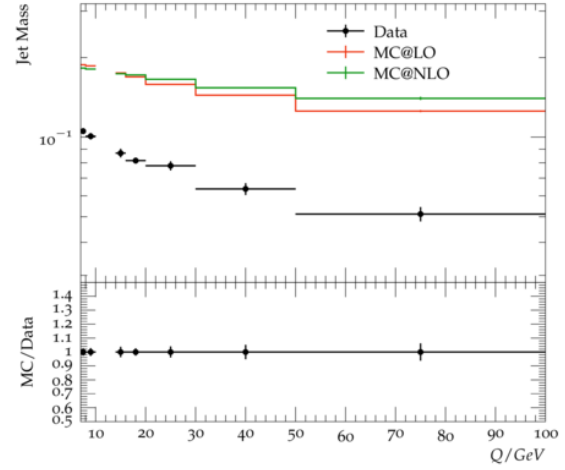
(a)



(b)



(c)



(d)

Figure 29: Herwig 7.2.1 simulation for Thrust  $\langle 1 - T_C \rangle$ ,  $\langle 1 - T_G \rangle$  with respect to photon direction, jet broadening  $B_T$  with kinematics cuts are for the ranges (7,100) in  $Q/GeV$  and ( 0.05, 0.8) in elasticity.

## 8 Inclusive $\phi$ -meson production

The total content of quark in the proton is determined through the DIS experiment. But there still remains to more information of be known about the sea of quarks especially in terms of its flavour decomposition. The data compared here is from the study of  $\phi$  meson production[37] in neutral current DIS collisions.

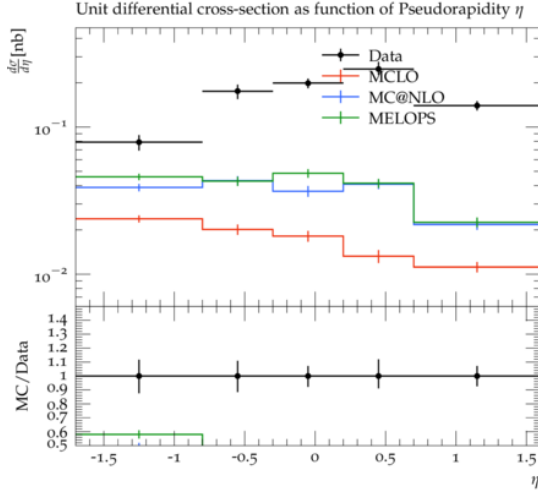
There are several processes involved in the production of  $\phi$ -meson. The  $\phi$  meson can be produced after the hadronisation of the strange quark from the strange sea of quarks inside proton after hard scattering off from an incoming photon which can be shown by  $\gamma^* s \rightarrow s$ . This hard scattering process can be modelled either through zeroth order QCD or the so-called Quark Parton Model (QPM) or through a first order interaction which is called the QCD Compton (QCDC) process. Apart from this hard scattering process. Another means of  $\phi$  meson production is through the boson gluon fusion (BGF),  $\gamma^* g \rightarrow ss$ . The main difference between this type of production and production of hard scattering is that, here the main dependency comes from the gluon density and is not dependent on the whether or not strange quarks are involved in the hard scattering. Instead the  $\phi$  mesons are produced from the strange quark produced in the hadronisation process. The other background process that can contaminate the data comes from diffractive scattering and from strange quarks produced from splitting of gluon which later hadronize or when a higher mass state like  $D_s$  decays into a  $\phi$ . Out of the main methods for studying strange particle processes are from the  $K^0$  mesons and baryons. Unlike these hadrons, which have contributions from higher mass state decays and fragmentation process, the  $\phi$  meson is sensitive to the strange quarks involved in the hard scattering process. They also have less contribution from the resonance decays. The contribution from QPM can also be improved by filtering for  $\phi$  mesons with high longitudinal momentum in the Breit frame.

The main signature for studying the  $\phi$  mesons produced comes from the  $\phi \rightarrow K^+ K^-$ . The Breit frame is the best when it comes to studying the system separated from the proton remnants. The photon in this frame is space-like with a four momentum,  $q = (0,0,0,-Q)$ . All the final state particles with transverse momentum in the Breit frame,  $p_{z_b} < 0$  are considered the current region and this particles are created from the fragmentation of the struck quark. All the remaining particles are called the target region.

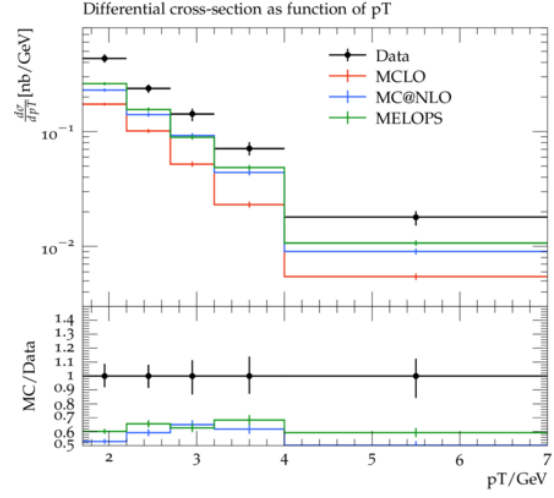
### 8.1 Kinematic selection

The data consists of measurements from the ZEUS detector, with  $\sqrt{s} = 300$  GeV. The kinematic region for data selection was restricted to the following requirement. The energy of the scattered lepton was required to be greater than,  $E_{e'} \geq 10$  GeV. The virtuality of the gauge boson, photon here, was required to be  $10 < Q_e^2 < 100$  GeV<sup>2</sup>. The maximum  $Q^2$  is limited to 100 to avoid complexities related to combinatorial background involved in the  $\phi$ -meson reconstruction.

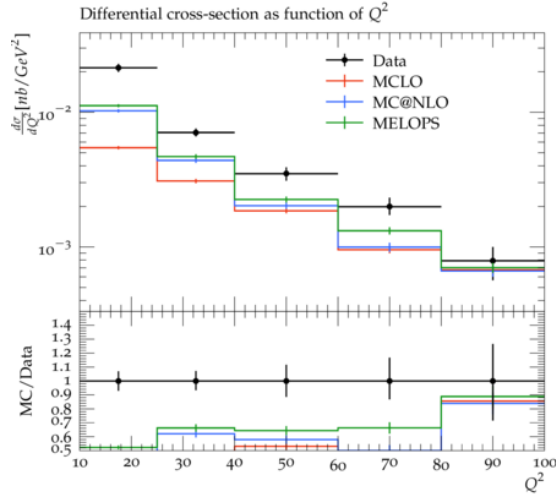
As mentioned earlier, the  $\phi$  candidates are identified from the charged Kaon pairs. The restriction on the tracks for the transverse momenta to be  $p_T > 200$  MeV in the lab frame. Of these tracks all the ones satisfying the conditions are selected and the invariant mass calculated. For a successful candidate to be selected the requirement is,  $0.99 < M(K^+ K^-) < 1.06$  GeV. The restrictions on the transverse momentum and pseudorapidity of the  $\phi$  meson in the lab frame were,  $p_T^\phi > 1.7$  GeV and  $-1.7 < \eta^\phi < 1.6$ .



(a)

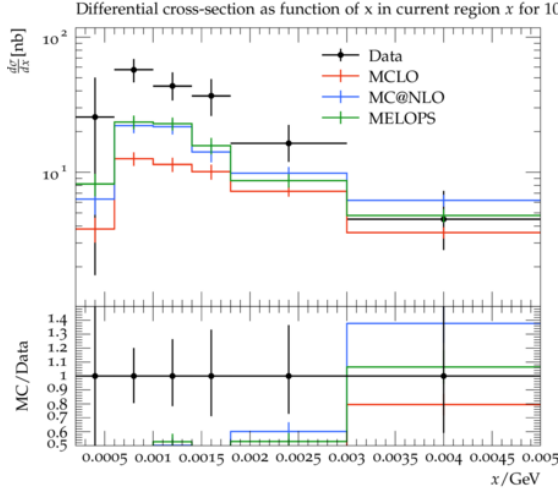


(b)

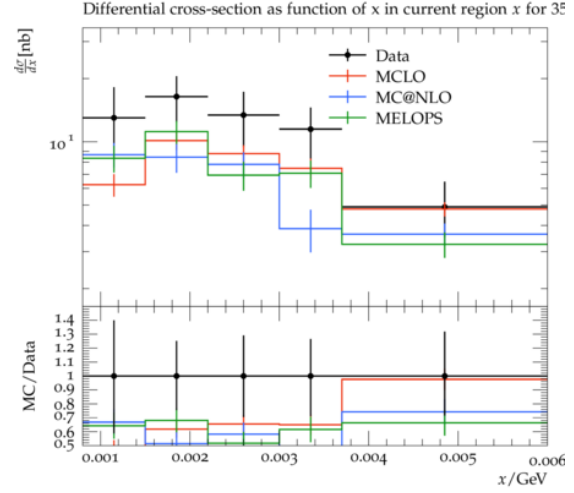


(c)

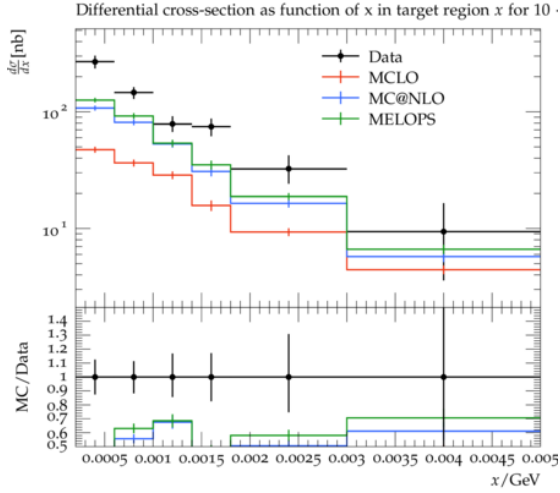
Figure 30: Sherpa 2.2.10 : Differential  $\phi$ -meson cross sections as functions of  $p_T^\phi$ ,  $\eta^\phi$ ,  $Q^2$  and scaled momentum,  $x_P$ , compared to Sherpa in LO, NLO and LO+Jet Matching simulations. The cross sections were measured in the kinematic region  $10 < Q^2 < 100 \text{ GeV}^2$ ,  $2 \cdot 10^4 < x < 10^2$ ,  $1.7 < p_T^\phi < 7 \text{ GeV}$  and  $1.7 < \eta_\phi < 1.6$ . The predictions are shown for  $\lambda_s = 0.22$ .



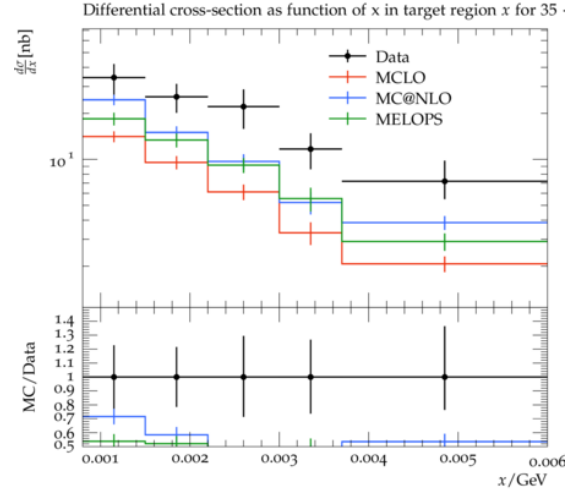
(a)



(b)



(c)



(d)

Figure 31: The inclusive sections as a function of bjorken  $x$  for two  $Q^2$  intervals,  $(35 < Q^2 < 100 \text{ GeV}^2)$  and  $(10 < Q^2 < 35 \text{ GeV}^2)$ , for the current, a)-b), and the target, c)-d), regions of the Breit frame compared to the LO,NLO and LO+ Jet Matching for Sherpa with predictions for  $\lambda_s = 0.22$ .

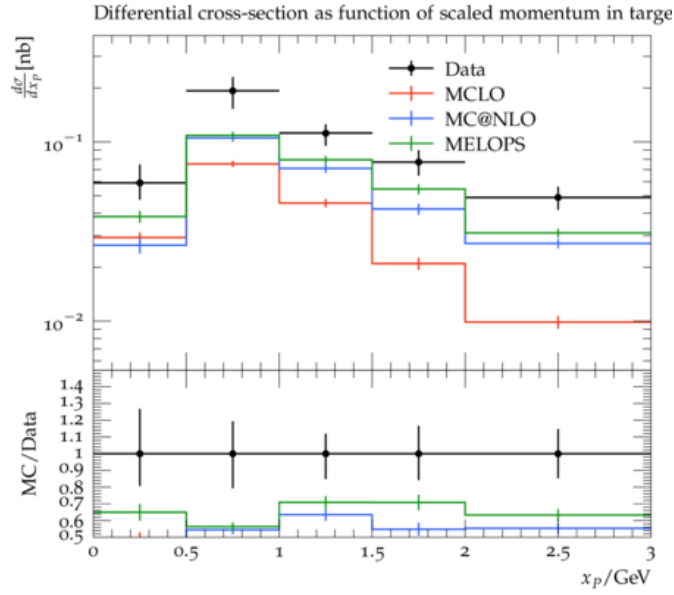
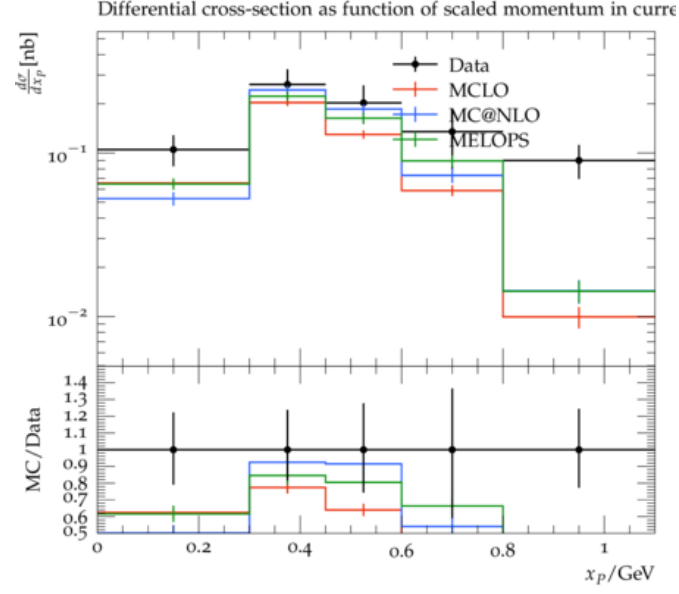


Figure 32: The inclusive sections as a function of  $x$  for two  $Q^2$  intervals, (  $35 < Q^2 < 100 \text{ GeV}^2$  ) and (  $10 < Q^2 < 35 \text{ GeV}^2$  ).





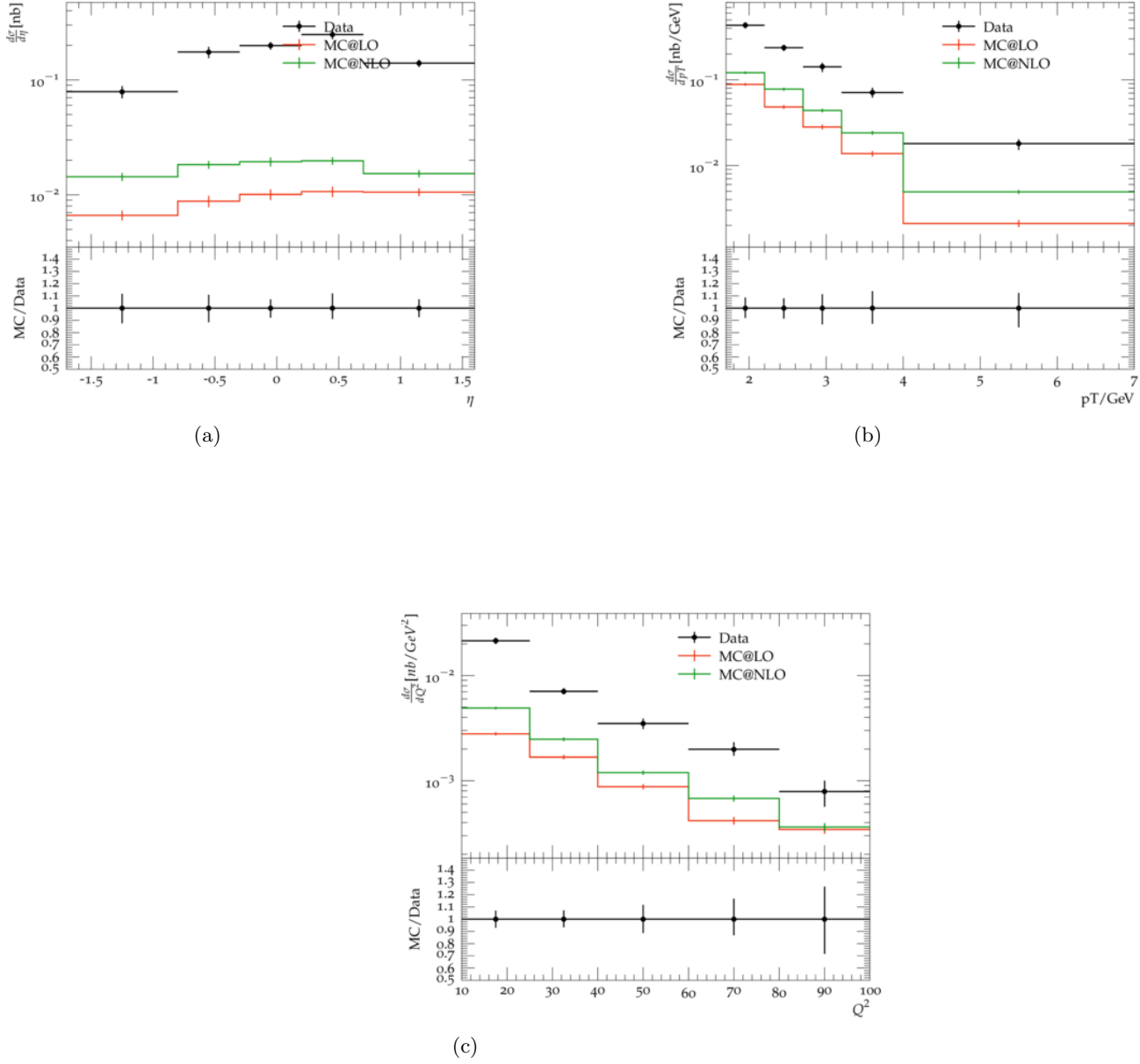
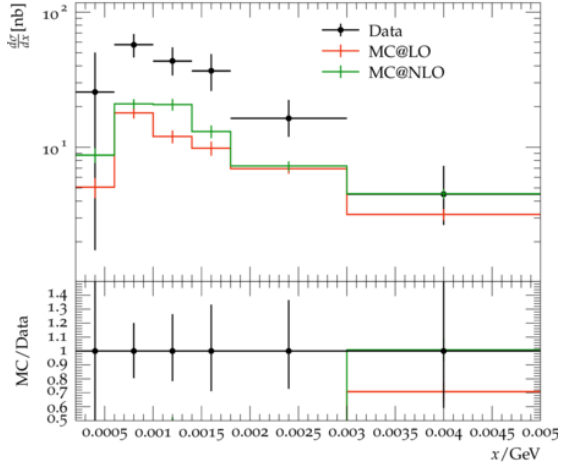
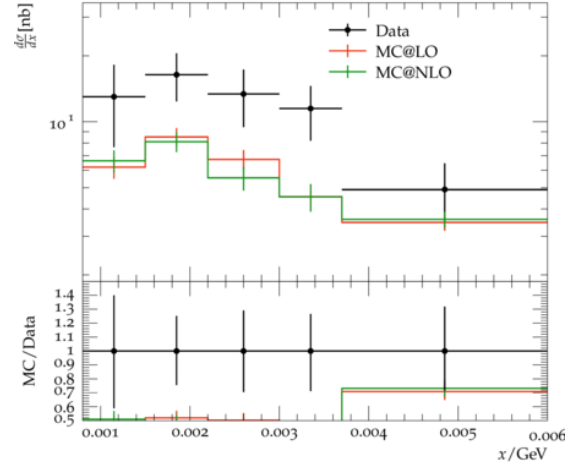


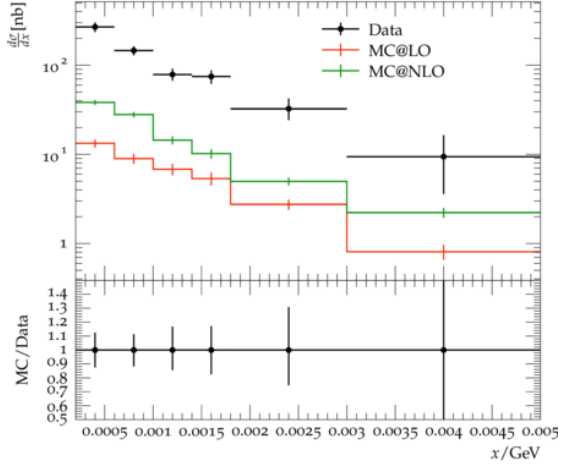
Figure 33: Herwig 7.2.1 : Differential  $\phi$ -meson cross sections as functions of  $p_T^\phi$ ,  $\eta^\phi$ ,  $Q^2$  and scaled momentum,  $x_P$ , compared to Sherpa in LO, NLO and LO+Jet Matching simulations. The cross sections were measured in the kinematic region  $10 < Q^2 < 100 \text{ GeV}^2$ ,  $2 \cdot 10^4 < x < 10^2$ ,  $1.7 < p_T^\phi < 7 \text{ GeV}$  and  $1.7 < \eta_\phi < 1.6..$  The predictions are shown for  $\lambda_s = 0.22$ .



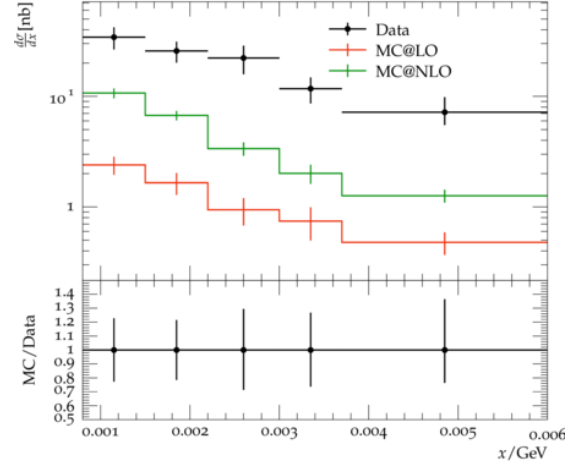
(a)



(b)

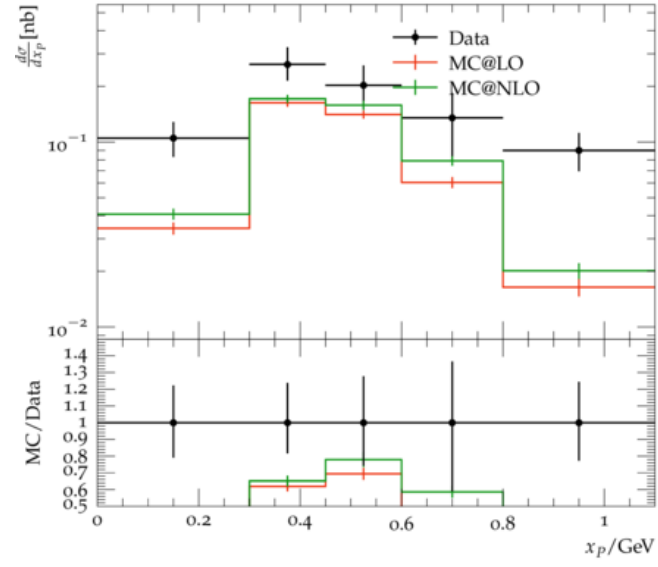


(c)

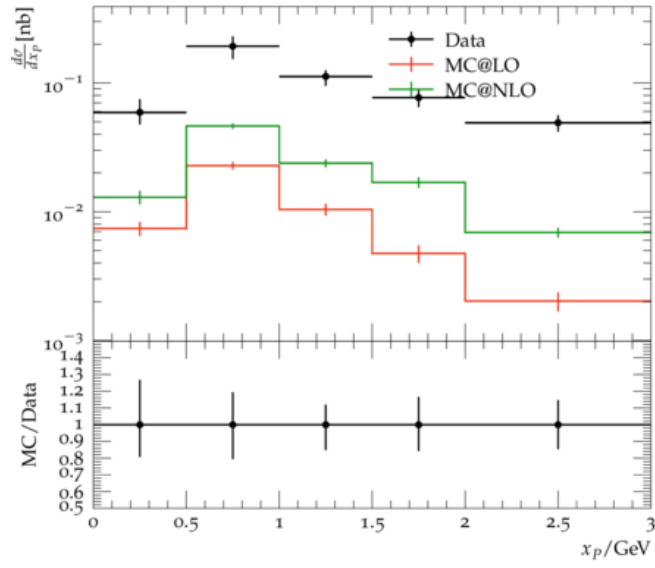


(d)

Figure 34: The inclusive sections as a function of bjorken  $x$  for two  $Q^2$  intervals, ( $35 < Q^2 < 100 \text{ GeV}^2$ ) and ( $10 < Q^2 < 35 \text{ GeV}^2$ ), for the current, a)-b), and the target, c)-d), regions of the Breit frame compared to the LO,NLO and LO+ Jet Matching for Sherpa with predictions for  $\lambda_s = 0.22$ .



(a)



(b)

Figure 35: The inclusive sections as a function of  $x$  for two  $Q^2$  intervals, ( $35 < Q^2 < 100 \text{ GeV}^2$ ) and ( $10 < Q^2 < 35 \text{ GeV}^2$ ).

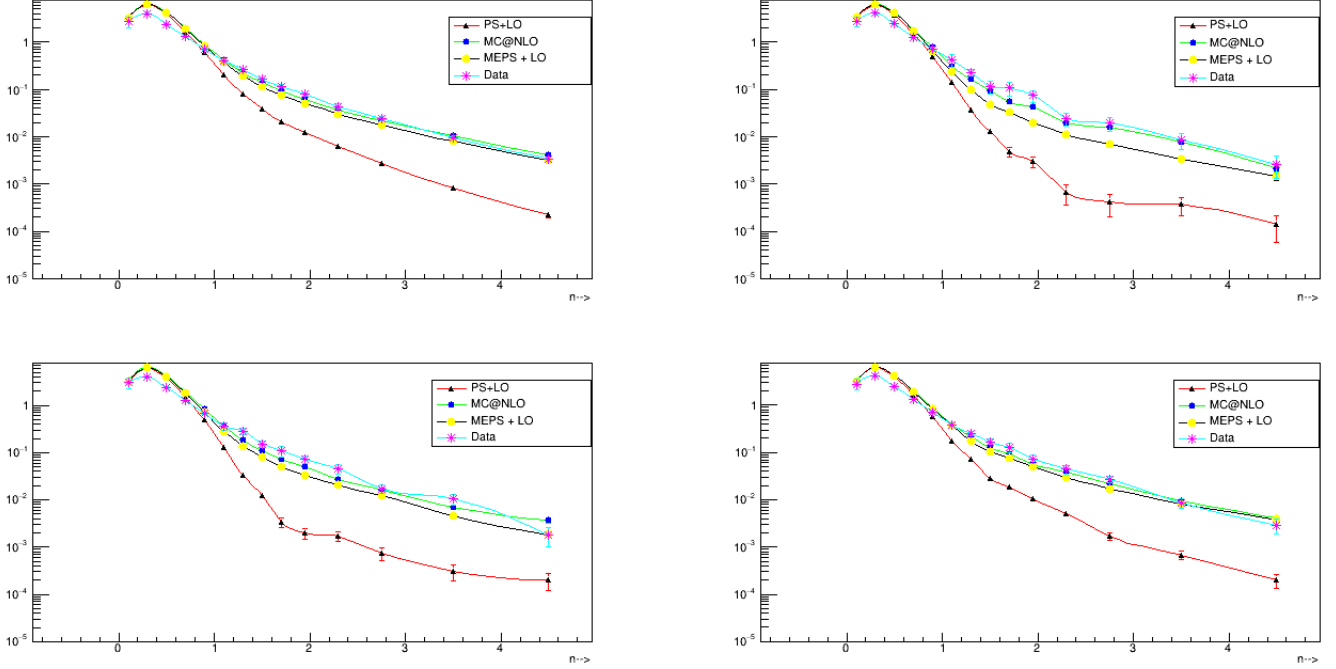


Figure 36: Transverse momentum spectra of charged particles in deep inelastic scattering are measured as a function of  $x_B$  and  $Q^2$  in the current and the central fragmentation regions.

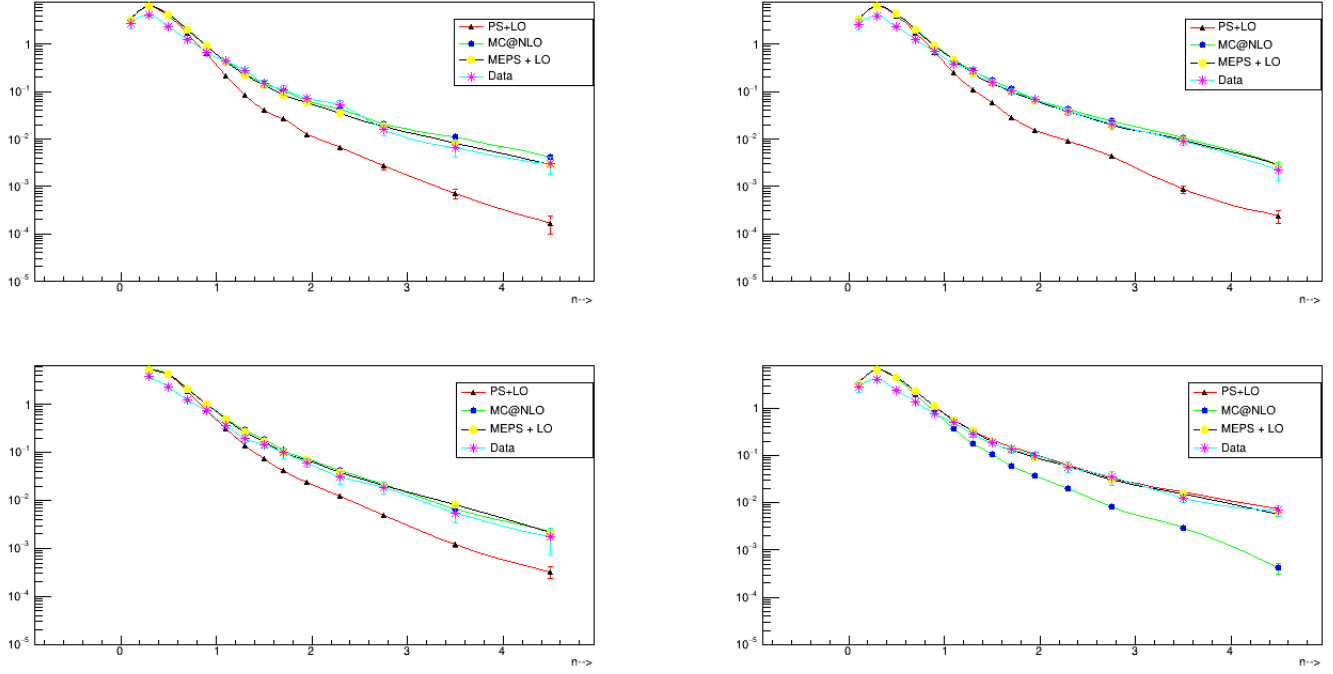


Figure 37: Charged Particle transverse momenta in respective bins of  $Q^2$  and Bjorken scaling 'x'

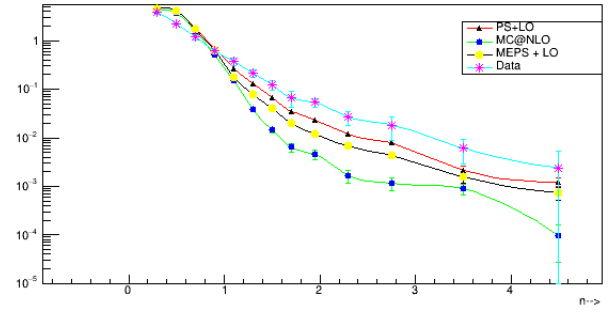
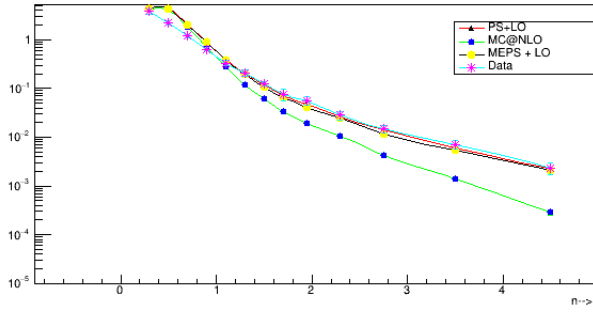
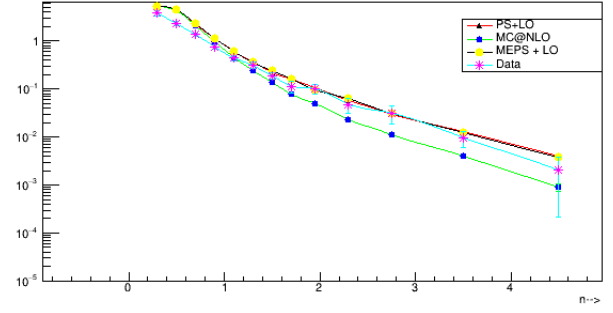
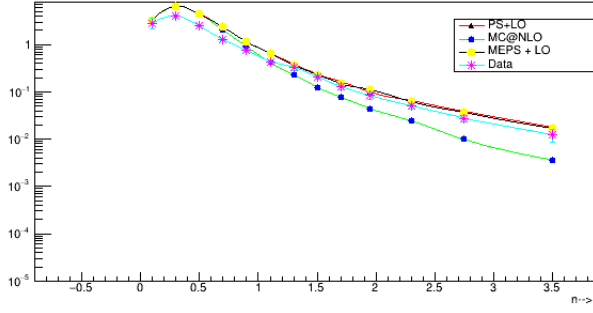


Figure 38

## 9 Diffractive Dijet Production in ep Collisions at HERA

In diffractive processes such as  $ep \rightarrow eXY$  in electron-proton collisions, (where the outgoing hadronic systems  $X$  and  $Y$ , are separated by large rapidity gap), the interacting hadrons either remain intact or dissociate into low mass hadronic systems via an exchange of pomeron (which has vacuum quantum numbers). The H1 experiment was equipped with two dedicated detectors, the Forward Proton Spectrometer (FPS) and the Very Forward Proton Spectrometer (VFPS) to detect diffractive events by identifying a large rapidity gaps in the rapidity distribution of the outgoing hadrons or by detecting a leading proton in the final state. The dijets production in diffractive deep inelastic scattering (DIS) and hard diffractive photoproduction ( $Q^2 \approx 0$ ) were studied in detail at HERA.

### 9.1 Diffractive Dijet photoproduction in ep collisions compared with H1 experiment

In this MC-Data comparison, PYTHIA8 was used and with following event selections ( H1\_2007\_I746380, arXiv:1502.01683)

- Beam energies of the proton & positron are 920 GeV and 27.5 GeV resp.
- $Q^2 < 2 \text{ GeV}^2$  and  $0.2 < y < 0.7$
- $0.010 < x_P < 0.024$ ,  $z_P < 0.8$  and  $|t| < 0.6 \text{ GeV}^2$
- $E_T^{jet1} > 5.5 \text{ GeV}$ ,  $E_T^{jet2} > 4.0 \text{ GeV}$  and  $-1 < \eta^{jet} < 2.5$

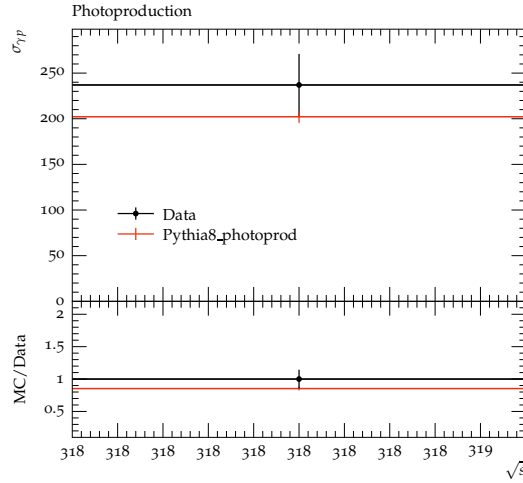
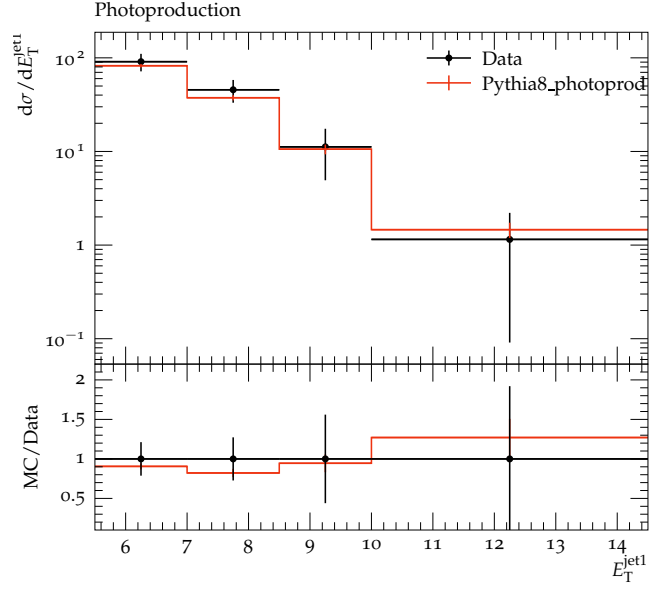
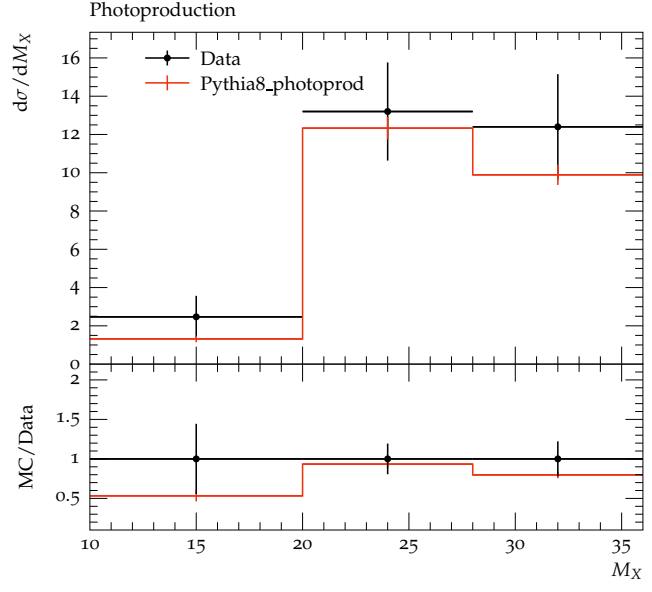


Figure 39: The cross-section for photoproduction

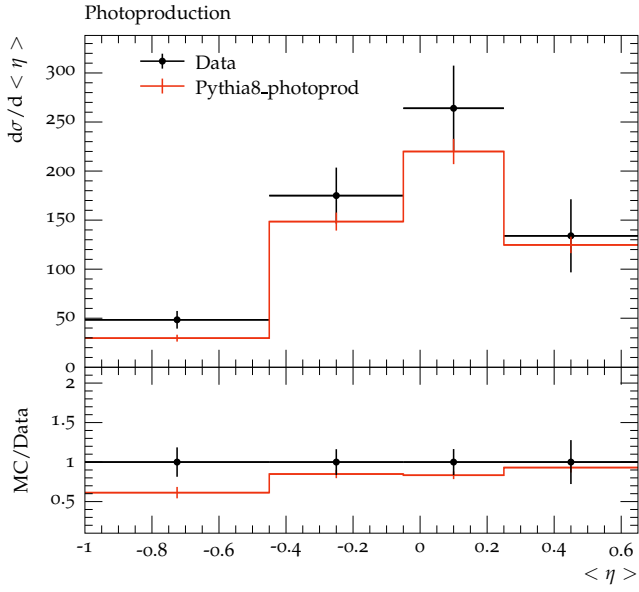




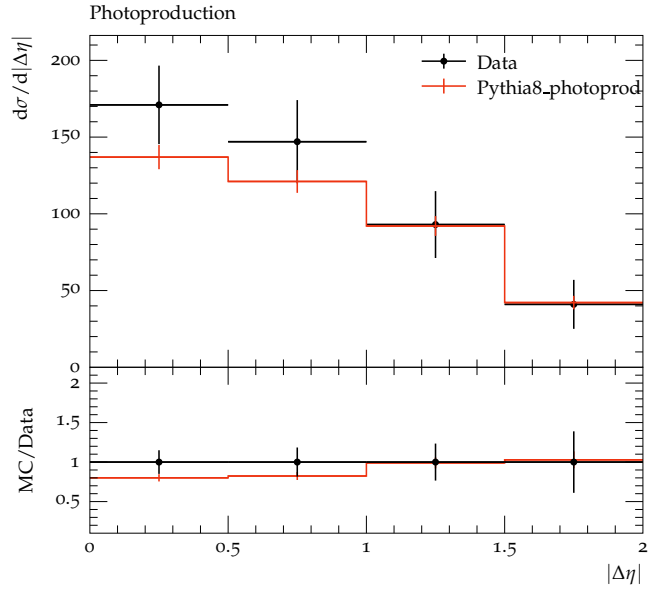
(a)



(b)

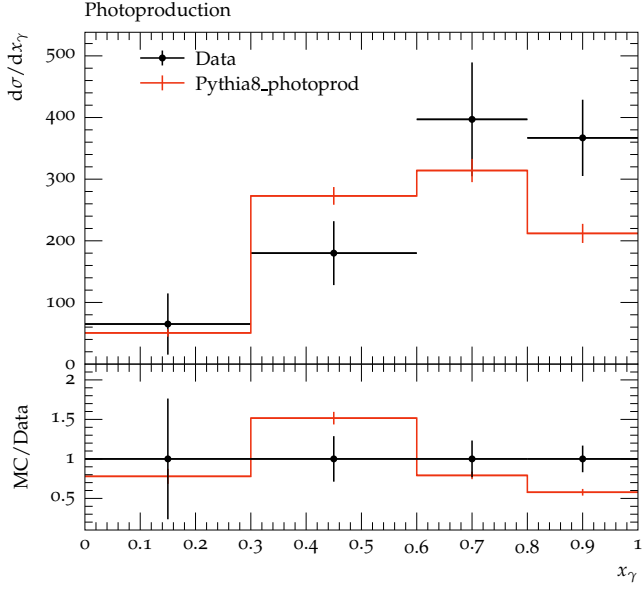


(c)

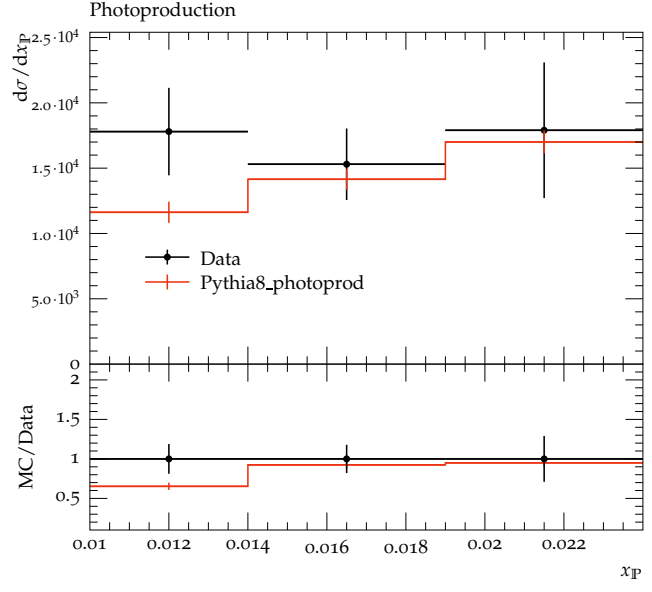


(d)

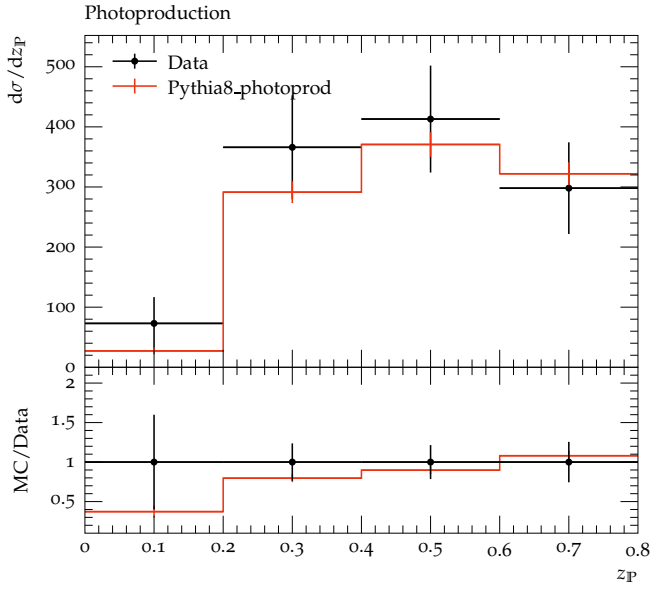
Figure 40: The diffractive dijet photoproduction in H1



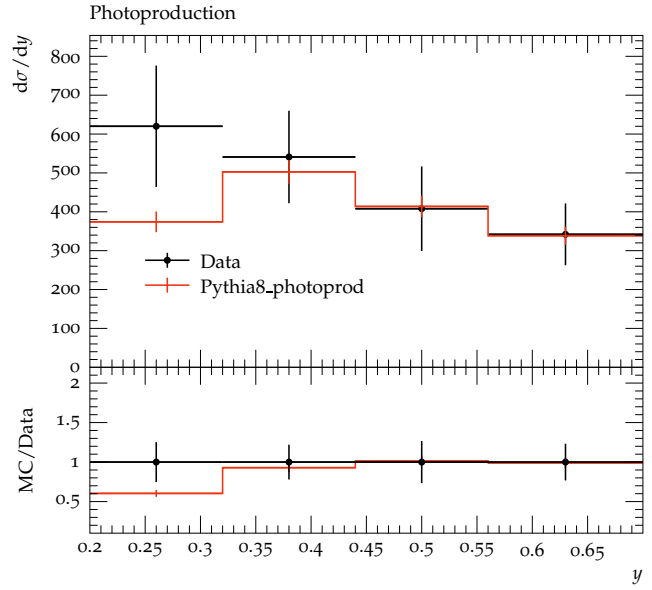
(a)



(b)



(c)



(d)

Figure 41: The diffractive dijet photoproduction in H1

## 9.2 Diffractive Dijet photoproduction in ep collisions compared with ZEUS experiment

In this MC-Data comparison, PYTHIA8 was used and with following event selections ( ZEUS\_2008\_I763404, arXiv:1502.01683)

- Beam energies of the proton & positron are 920 GeV and 27.5 GeV resp.
- Total integrated luminosity is  $77.2 \text{ pb}^{-1}$  (ZEUS)
- Generated 1.5 M PYTHIA8 events for comparison
- $Q^2 < 1 \text{ GeV}^2$  and  $0.2 < y < 0.85$
- $x_P < 0.025$
- $E_T^{jet1} > 7.5 \text{ GeV}$ ,  $E_T^{jet2} > 6.5 \text{ GeV}$  and  $-1.5 < \eta^{jet} < 1.5$

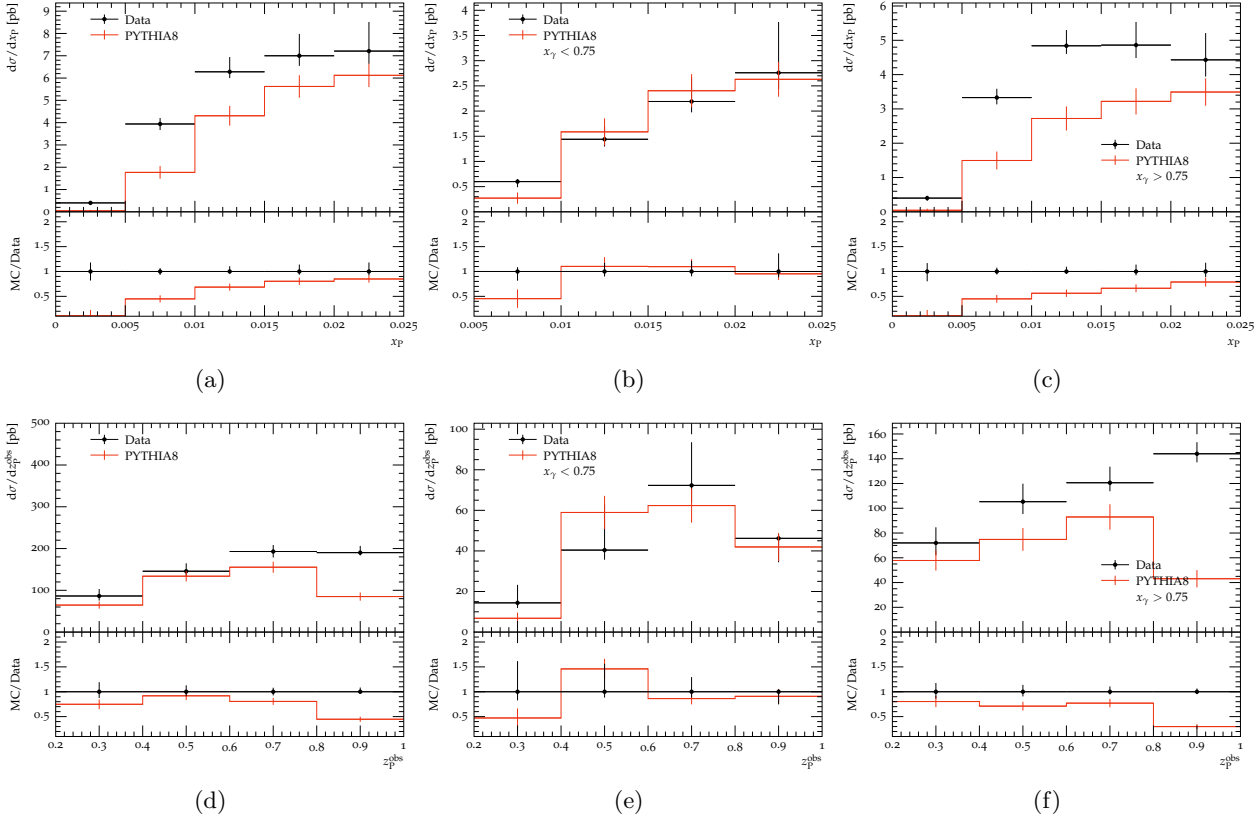


Figure 42: The diffractive dijet photoproduction in ZEUS

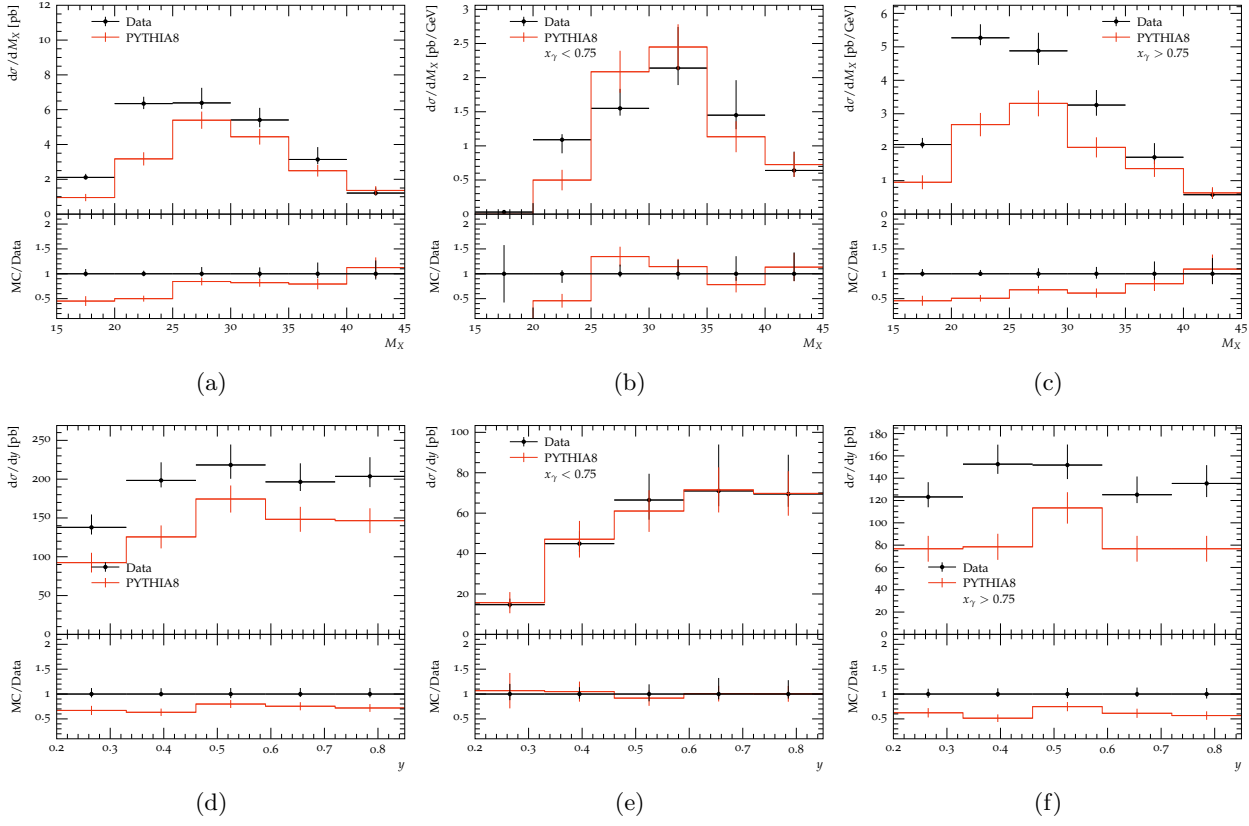
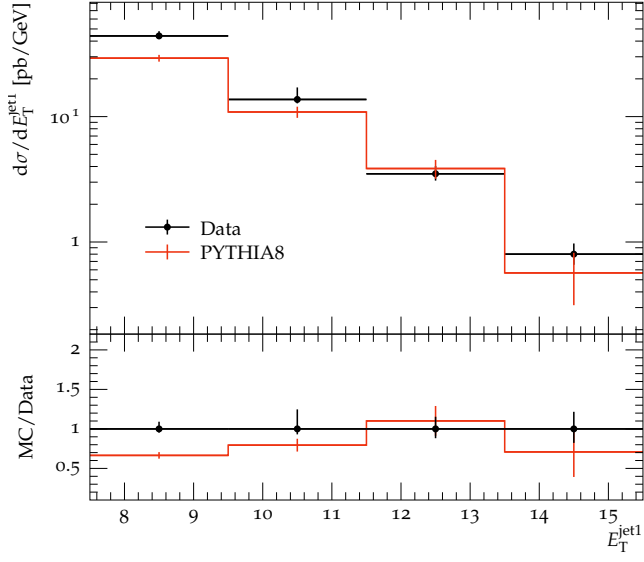
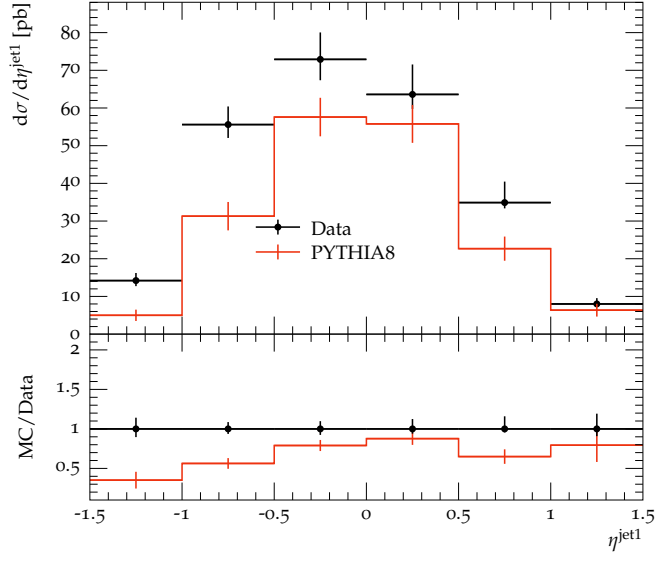


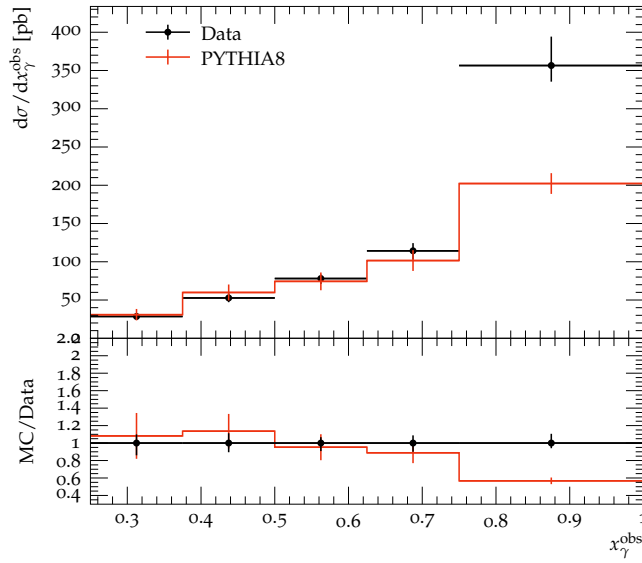
Figure 43: The diffractive dijet photoproduction in ZEUS



(a)



(b)



(c)

Figure 44: The diffractive dijet photoproduction in ZEUS

### 9.3 Tests of QCD Factorisation in the Diffractive Production of Dijets in Photoproduction at HERA

In this section, MC-Data comparison of dijets Photoproduction at H1 (H1\_2007\_I746380) arXiv:0703022 with PYTHIA8 is discussed.

Following are some of the event selections implemented in the analyses.

- Beam energies of the proton & positron are 820 GeV and 27.5 GeV respectively
- $Q^2 < 0.01 \text{ GeV}^2$  and  $165 < W_{\gamma p} < 242$
- $0.010 < x_P < 0.03$ ,  $M_Y < 1.6 \text{ GeV}$  and  $|t| < 1.0 \text{ GeV}^2$
- $E_T^{jet1} > 5.0 \text{ GeV}$ ,  $E_T^{jet2} > 4.0 \text{ GeV}$  and  $-1 < \eta^{jet} < 2.0$

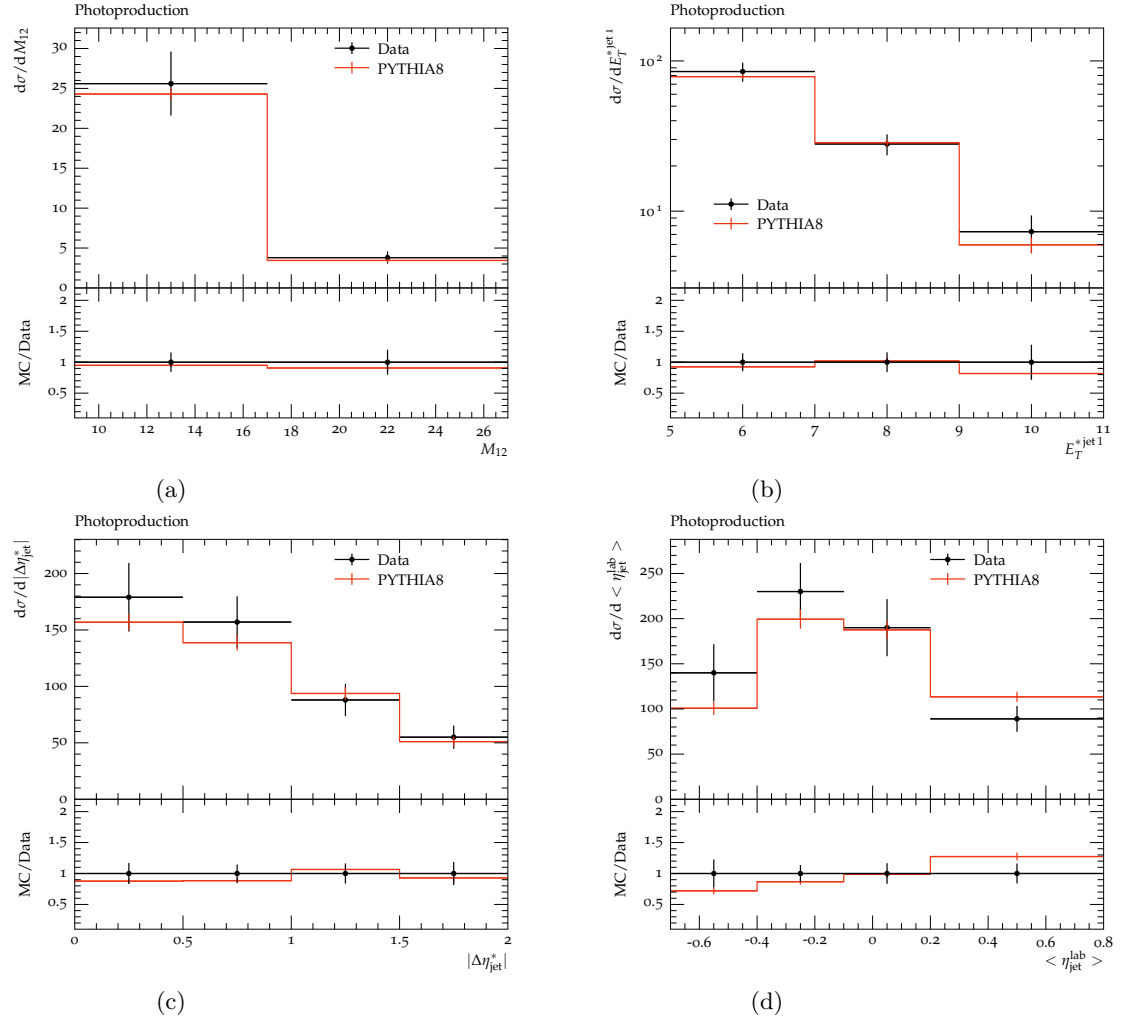
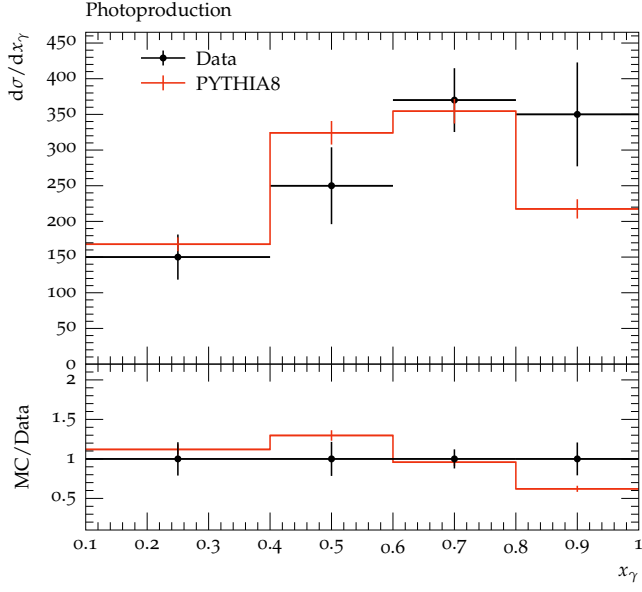
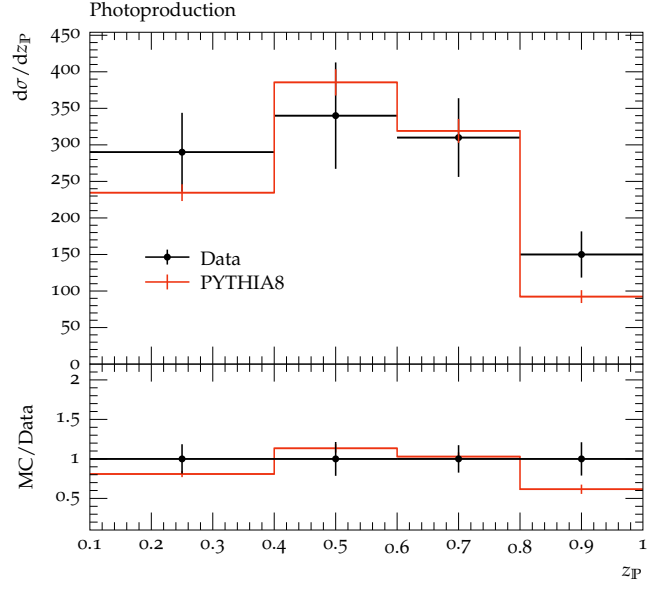


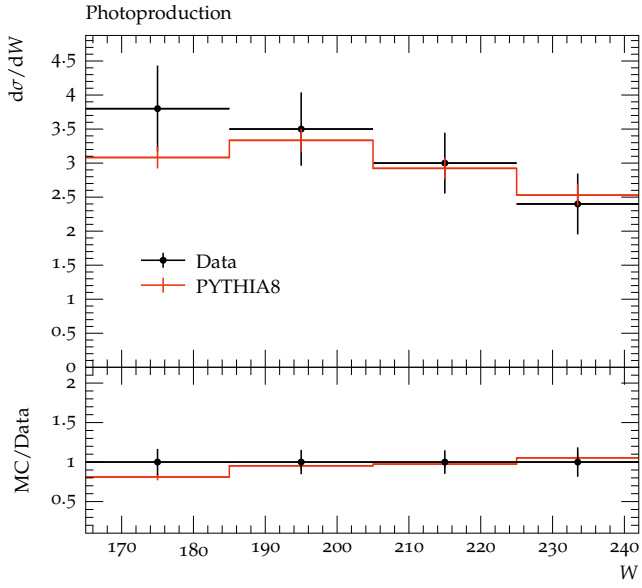
Figure 45: The diffractive dijet photoproduction in H1



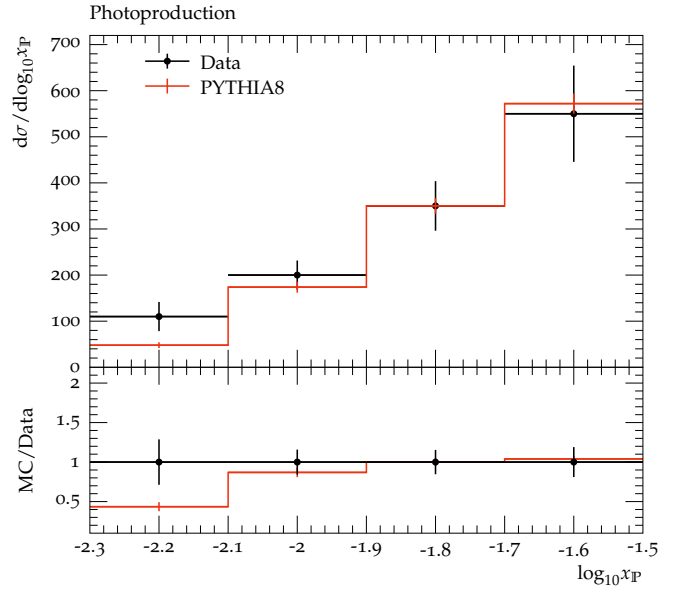
(a)



(b)



(c)



(d)

Figure 46: The diffractive dijet photoproduction in H1

## 10 Inclusive-jet photoproduction at HERA

Inclusive-jet photoproduction have been measured in the  $ep \rightarrow e + jet + X$  in electron-proton collisions (where  $X$  is the outgoing hadronic systems). In this MC-Data comparison, PYTHIA8 was used and with following event selections.

- Comparison of Inclusive jet production at ZEUS (ZEUS\_2012\_I1116258) arXiv:1205.6153 with Pythia8
- Beam energies of the proton & positron are 920 GeV and 27.5 GeV resp.
- Total integrated luminosity is  $300 \text{ pb}^{-1}$  (ZEUS) and 1.0 M PYTHIA8 events
- $Q^2 < 1 \text{ GeV}^2$ ,  $0.2 < y < 0.85$ , and  $142 < W_{\gamma p} < 293 \text{ GeV}$
- $E_T^{jet} > 17 \text{ GeV}$  and  $-1.0 < \eta^{jet} < 1.5$
- $x$  region covered by the measurements is  $0.003 < x < 0.95$

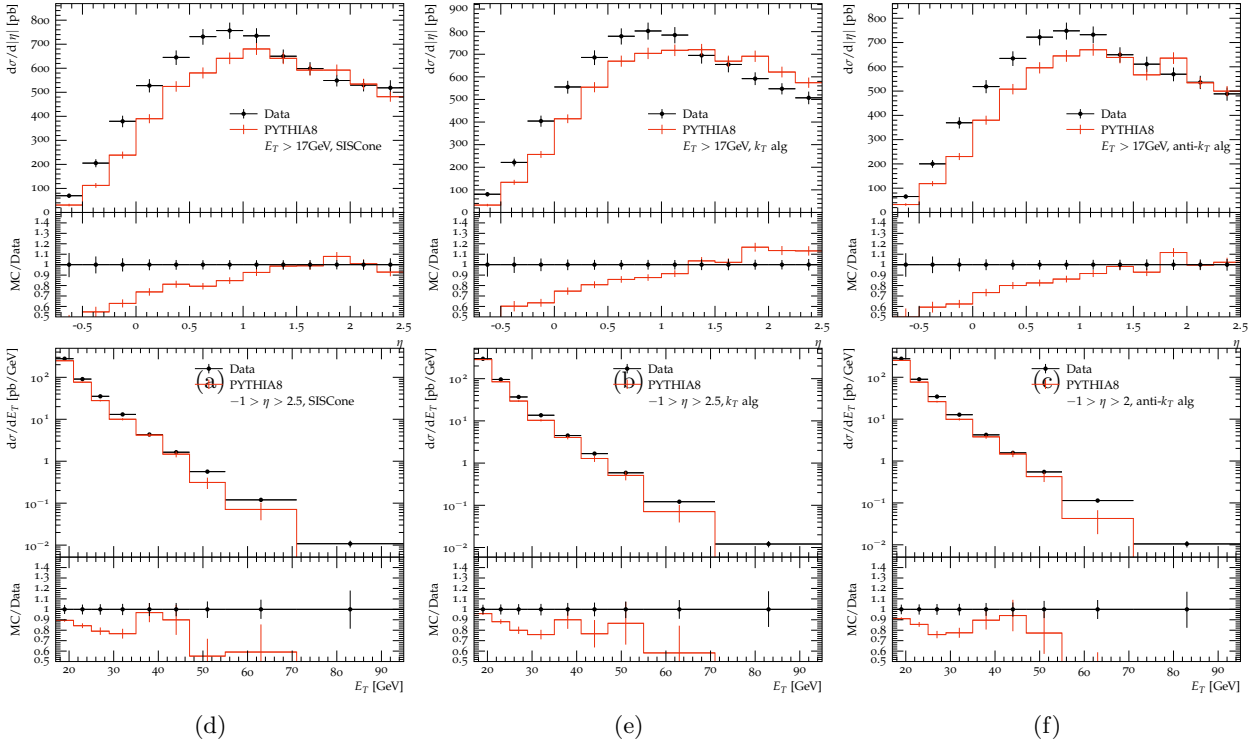


Figure 47: The inclusive jet production in ZEUS



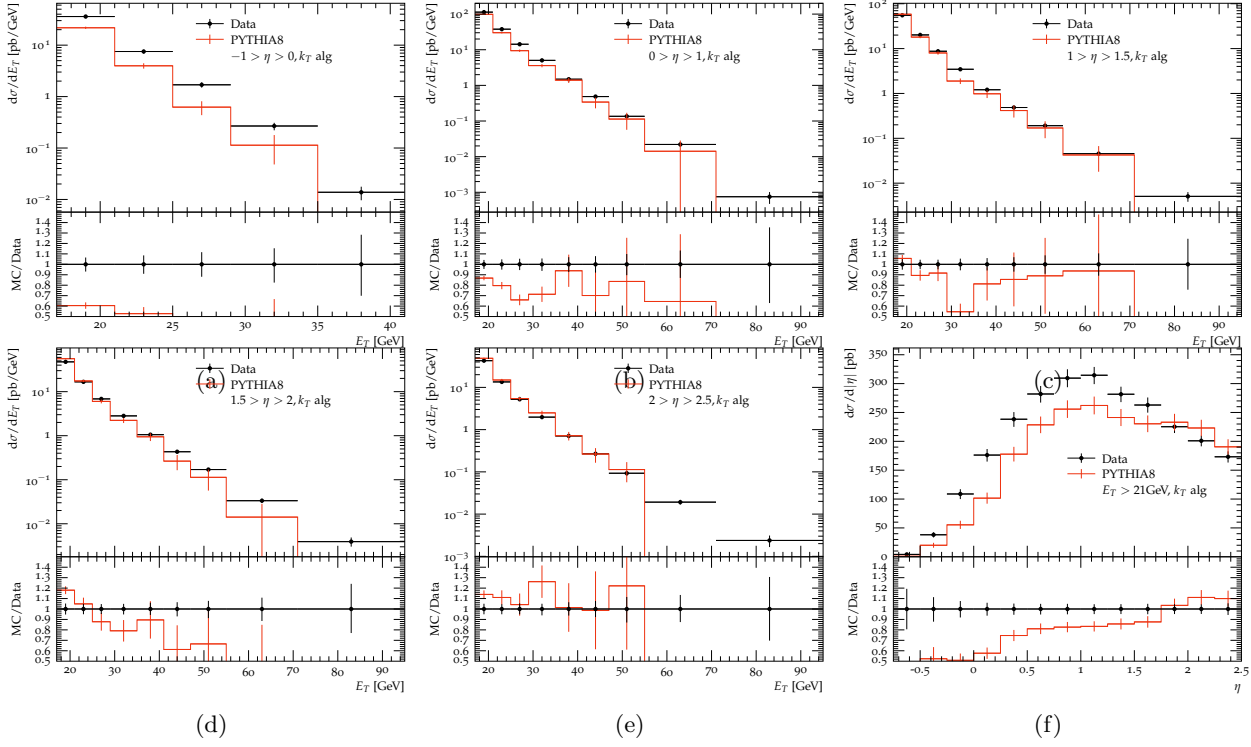


Figure 48: The inclusive jet production in ZEUS

## 11 Summary

Interpretation of the comparisons and next steps

## 12 RIVET and MC Generator tools and Usage

### 12.1 RIVET

The RIVET tool comes in a standalone or docker container-type version. The Docker container is easier to install; hence it has been used for all of our studies. There is more than one docker container. The one regularly updated is the docker pull `hepstore/rivet`. Other docker images such as `docker pull hepstore/rivet-pythia` can also be used for data sets from a specific generator. Although the RIVET guide contains all the necessary instructions, below, we have provided guidelines that were used in our analyses.

#### SET-UP and RUN

The first task is to get a `hepmc` file from your Monte Carlo generator and the docker image of the RIVET container you require, using the docker pull command. The setup of the container can be achieved using the following commands.

- `$ alias rivet='docker run -i -rm -u 'id -u $USER':'id -g' -v $PWD:$PWD -w $PWD hepstore/rivet rivet'`
- `$ alias rivet-mkhtml='docker run -i -rm -u 'id -u $USER':'id -g' -v $PWD:$PWD -w $PWD hepstore/rivet rivet-mkhtml'`
- `$ alias make-plots='docker run -i -rm -u 'id -u $USER':'id -g' -v $PWD:$PWD -w $PWD hepstore/rivet make-plots'`

Next, identify the standard RIVET analysis to be implemented. Then run the following commands. If `dis` is the file name and `-a H1-1994-S2919893` is the analysis, then

- `$ rivet dis.hepmc -a H1-1994-S2919893`  
This will generate a `Rivet.yoda` file in your working directory. The comparison plots can be produced with the next command.
- `$ rivet-mkhtml Rivet.yoda`  
If there are multiple yoda files, they can all be compared together in the following manner.
- `$ rivet-mkhtml dis1.yoda dis2.yoda dis3.yoda`  
The previous two commands will automatically generate a directory named `rivet-plots` containing images as well as `.dat` files of the comparison plots. Any changes to these plots can be achieved through changes made to their `.dat` files, followed by,
- `$ make-plots a1.dat`

Use this link for further information on usage of `make-plots` in `rivet`.

#### BUILDING NEW ANALYSIS

If a non-standard analysis is to be implemented, the analysis has to be built and compiled in the following manner. Along with the first three commands given in this section, use the following two as well.

- `$ USER:'id -g' -v $PWD:$PWD -w $PWD hepstore/rivet rivet-mkanalysis'`
- `$ alias rivet-build='docker run -i -rm -u 'id -u $USER':'id -g' -v $PWD:$PWD -w $PWD hepstore/rivet rivet-build'`  
Followed by,
- `$ rivet-mkanalysis new-analysis`  
This will create a RIVETnew-analysis.so and new-analysis.cc files.  
Open the .cc file and write the code, then,
- `$ rivet-build RIVETnew-analysis.so RIVETnew-analysis.cc`
- `rivet -list-analyses -pwd`  
checks if your local analysis is ready for use
- `rivet dis.hepmc -a new-analysis -pwd`  
do not forget the `-pwd` tag while running local analysis.

For more information of RIVET tool, refer to the Rivet website or EIC-User group tutorials.

## 12.2 Pythia8

EIC group used both the docker container as well as a standalone version of Pythia8. Among the MCs, Pythia8 standalone is the easiest to set up and implement. The documentation for standalone is well maintained by the developers with rarely any bugs.

The Pythia8 docker container setup is described below.

`$ docker pull electronioncollider/escalate`

this escalate version of pythia automatically comes with dire-shower enabled in it, use the electronioncollider/pythia-eic-tutorial docker

image(rivet-enabled) if required otherwise, or the standalone pythia8.

Next Steps:

- `docker run -it -rm -p8888:8888 -p 6080:6080 electronioncollider/escalate`  
or,
- `docker run -it -rm -p8888:8888 electronioncollider/escalate` ,in case previous one does not work.  
In the jupyter-lab window go to the 01-fast-sim-tutorial/5-pythia8-dire.ipynb file.

Running this code file by inputting the required beam and other parameters, generates a hepmc file that can be downloaded to your local system and, fed into RIVET for further analyses and comparison. Certain DIS parameters are also available inside dis-hera.cmnd file in the jupyter-lab. Ensure that the beam parameters match the Rivet-analyses parameters.

The Standalone Pythia8 allows wider usage and can be configured to generate a hepmc or root file output. The setup information is available with all details on the MC web-page.

## 12.3 Herwig7

Using standalone Herwig7 requires configuration with hepmc and other important packages separately. A docker container is very useful with everything inbuilt, including Rivet, though it takes quite a bit of time to finish one single simulation run. Following are the instructions for the setup.

```
$ docker pull graemenail/herwig-eic
```

Also, download these input files , and work in the directory containing these files.

- `$ alias Herwig='docker run -i -rm -u $(id -u $USER):$(id -g) -v $PWD:$PWD -w $PWD graemenail/herwig-eic Herwig'`
- `$ alias rivet-mkhtml='docker run -i -rm -u $(id -u $USER):$(id -g) -v $PWD:$PWD -w $PWD graemenail/herwig-eic rivet-mkhtml'`

The DIS-Matchbox.in is the input file for the required analysis. The next two commands will generate 10k DIS events. Before which open the DIS-Matchbox.in and check for beam parameters and other specifics.

- Herwig read DIS-Matchbox.in
- Herwig run -N 10000 DIS-Matchbox.run

Any modifications to beam parameters, Parton showers, etc can be done through the DIS-Matchbox.in file. To enable hepmc and rivet, add/uncomment the following lines inside DIS-Matchbox.in file.

```
cd /Herwig/Analysis
insert Rivet:Analyses 0 H1_2000_S41291303
insert /Herwig/Generators/EventGenerator:AnalysisHandlers 0 Rivet
insert /Herwig/Generators/EventGenerator:AnalysisHandlers 0 HepMC
```

Above code lines will directly give the hepmc and yoda files outputs, based on the rivet analyses fed to it.

- `$ rivet-mkhtml DIS-Matchbox.hepmc` , will give the comparison plots.

## 12.4 Sherpa2

Similar to Herwig7 and Pythia8, the docker container of Sherpa2 is better to configure and use, compared to the standalone version, which requires additional configuration and installations.

The docker container and input files can be obtained from;

```
$ docker pull sherpamc/sherpa:2.2.7 and
```

```
$ git clone https://gitlab.com/shoeche/tutorials.git
```

respectively. The guide attached with the git-cloned folder contains several required instructions.

Set up and open the sherpa bash with;

- `$ docker run -it -u $(id -u $USER) -rm -v $HOME:$HOME -w $PWD sherpamc/sherpa:2.2.7`  
Move to the tutorials/(the directory that was git-cloned) and,
- `cd rivet`

- rivet-buildplugin MC-TTBar.cc
- cp RivetAnalysis.so ../mc/sherpa/

Open The Run.dat file and use the following code to generate leading order events in Sherpa (MEPS and NLO codes can be obtained from the EICUG tutorial)

Event Generation: Open the Run.dat file, add following code:

```
(run)
{BEAM_1 -11 27.6; BEAM_2 2212 920
RESPECT_MASSIVE_FLAG 1; PDF_SET_1 None;
SCALES VAR{-Abs2(p[0]-p[2])} }
(run)

(processes)
{Process -11 93 - > -11 93
End process
}(processes)

(selector){
Q2 -11 -11 150 1e5
}(selector)

(analysis){
BEGIN_RIVET
H1_2000.S41291303
USE_HEPMC_SHORT 1
END_RIVET
}(analysis)
```

Then in the sherpa bash, run

- \$ Sherpa -aRivet -e10k for 10k events  
you will directly get a .yoda output based on the analysis mentioned in Run.dat file)  
For generating a hepmc, run
- \$ Sherpa -e10k EVENT\_OUTPUT=HepMC\_Short[events\_1j]

## References

- [Bie+20a] Christian Bierlich et al. “Confronting experimental data with heavy-ion models: RIVET for heavy ions”. In: *Eur. Phys. J. C* 80.5 (2020), p. 485. DOI: 10.1140/epjc/s10052-020-8033-4. arXiv: 2001.10737 [hep-ph].
- [Bie+20b] Christian Bierlich et al. “Robust Independent Validation of Experiment and Theory: Rivet version 3”. In: *SciPost Phys.* 8 (2020), p. 026. DOI: 10.21468/SciPostPhys.8.2.026. arXiv: 1912.05451 [hep-ph].

- [BR19] Christian Bierlich and Christine O. Rasmussen. “Dipole evolution: perspectives for collectivity and  $\gamma^*A$  collisions”. In: *JHEP* 10 (2019), p. 026. DOI: 10.1007/JHEP10(2019)026. arXiv: 1907.12871 [hep-ph].
- [Bie+18] Christian Bierlich et al. “The Angantyr model for Heavy-Ion Collisions in PYTHIA8”. In: *JHEP* 10 (2018), p. 134. DOI: 10.1007/JHEP10(2018)134. arXiv: 1806.10820 [hep-ph].
- [Buc+21] Andy Buckley et al. “The HepMC3 event record library for Monte Carlo event generators”. In: *Comput. Phys. Commun.* 260 (2021), p. 107310. DOI: 10.1016/j.cpc.2020.107310. arXiv: 1912.08005 [hep-ph].
- [CS18] Baptiste Cabouat and Torbjörn Sjöstrand. “Some Dipole Shower Studies”. In: *Eur. Phys. J. C* 78.3 (2018), p. 226. DOI: 10.1140/epjc/s10052-018-5645-z. arXiv: 1710.00391 [hep-ph].
- [Fis+16] Nadine Fischer et al. “Vincia for Hadron Colliders”. In: *Eur. Phys. J. C* 76.11 (2016), p. 589. DOI: 10.1140/epjc/s10052-016-4429-6. arXiv: 1605.06142 [hep-ph].
- [Hel18] Ilkka Helenius. “Photon-photon and photon-hadron processes in Pythia 8”. In: *CERN Proc.* 1 (2018). Ed. by David d’Enterria, Albert de Roeck, and Michelangelo Mangano, p. 119. DOI: 10.23727/CERN-Proceedings-2018-001.119. arXiv: 1708.09759 [hep-ph].
- [HR19] Ilkka Helenius and Christine O. Rasmussen. “Hard diffraction in photoproduction with Pythia 8”. In: *Eur. Phys. J. C* 79.5 (2019), p. 413. DOI: 10.1140/epjc/s10052-019-6914-1. arXiv: 1901.05261 [hep-ph].
- [HP15] Stefan Höche and Stefan Prestel. “The midpoint between dipole and parton showers”. In: *Eur. Phys. J. C* 75.9 (2015), p. 461. DOI: 10.1140/epjc/s10052-015-3684-2. arXiv: 1506.05057 [hep-ph].
- [Sjö+15] Torbjörn Sjöstrand et al. “An introduction to PYTHIA 8.2”. In: *Comput. Phys. Commun.* 191 (2015), pp. 159–177. DOI: 10.1016/j.cpc.2015.01.024. arXiv: 1410.3012 [hep-ph].
- [Wau+06] B. M. Waugh et al. “HZTool and Rivet: Toolkit and Framework for the Comparison of Simulated Final States and Data at Colliders”. In: *15th International Conference on Computing in High Energy and Nuclear Physics*. May 2006. arXiv: hep-ph/0605034.